September 1974

To the Graduate Council:

I am submitting herewith a thesis written by Sung-I Juan entitled "Optical Properties of Nucleic Acid Bases in the Soft X-Ray Region." I recommend that it be accepted for nine quarter hours of credit in partial fulfillment of the requirements for the degree of Master of Science, with a major in Physics.

R O Barthoff

Major Professor

We have read this thesis
and recommend its acceptance:

M. J. Fair

R. J. Lovell

Accepted for the Council:

Stelton A. Smith

Vice Chancellor for
Graduate Studies and Research

B

OPTICAL PROPERTIES OF NUCLEIC ACID BASES IN THE SOFT X-RAY REGION

A Thesis

Presented to

the Graduate Council of

The University of Tennessee

In Partial Fulfillment

of the Requirements for the Degree

Master of Science

---

by

Sung-I Juan

March 1975

ACKNOWLEDGMENTS

The author would like to thank Drs. E. T. Arakawa, M. W. Williams, T. Inagaki and R. N. Hamm for many helpful discussions, for computer programming assistance by Dr. Hamm, for experimental assistance by Dr. L. C. Emerson and for the constant encouragement and guidance by Dr. R. D. Birkhoff.

This research was supported by the Oak Ridge National Laboratory which is operated by Union Carbide Corporation for the U. S. Atomic Energy Commission.

1197644

ABSTRACT

Optical properties are determined for the nucleic acid base adenine in the energy range from 2 to 82 eV and for thymine, cytosine and uracil in the energy range from 25 to 82 eV. The optical properties are calculated from experimentally measured reflectance. The reflectance is measured for thin films of the bases sublimed onto glass in a vacuum, and then exposed to the atmosphere while being transferred to the reflectance chamber where the reflectance measurements are made in vacuum. Normal incidence reflectance (R_n) measurements are directly measured in the energy range 4 to 33 eV for adenine and reflectance as a function of incident photon angle is measured in the energy range 33 to 82 eV for adenine and from 25 to 82 eV for the other bases. The reflectance as a function of angle of incidence data is fitted to Fresnel's equations to obtain n and k values from which R_n can be calculated for the Kramers-Kronig analysis. Below 4 eV the near-normal incidence reflectance is determined from interference effects, since the adenine film is transparent.

For adenine the near-normal incidence reflectance data are used in a Kramers-Kronig analysis and the complex refractive index $\tilde{n}$ and the complex dielectric constant ϵ obtained over the energy range measured. Whereas for adenine our data below 10 eV are compared with previously published data, our optical data above 10 eV are presented for the first time. The data for cytosine, thymine and uracil from 25 to 82 eV are presented for the first time.

Direct comparison of k, the imaginary part of $\tilde{n}$, gives good agreement with values from published transmission measurements made below 10 eV. Comparison of ϵ_2, the imaginary part of ϵ, is made with theoretically calculated energy transitions in molecular adenine. Acceptable agreement is observed here. The energy loss function, $-\mathrm{Im}(1/\epsilon)$, is compared with electron energy loss data. Good agreement is obtained at low energies and discrepancies at higher energies are attributed to film differences. A comparison of ϵ_2 and $-\mathrm{Im}(1/\epsilon)$ is made, and the results are related to collective oscillations of the loosely bound electrons in adenine.

TABLE OF CONTENTS

CHAPTER	PAGE
I. INTRODUCTION	1
Introduction	1
Review of Previous Work	3
Present Work	8
II. THEORY	10
Optical Constants	10
Reflectance	12
Kramers-Kronig analysis of the reflectance data	17
Sum rules	20
Energy loss function	21
Classical Dielectric Theory	22
Covalent Bonding	26
III. EXPERIMENTAL APPARATUS	29
Apparatus for Evaporation	29
Apparatus for Measuring the Optical Properties	30
IV. EXPERIMENTAL PROCEDURE AND DETERMINATION OF OPTICAL CONSTANTS	33
Substrate Cleaning	33
Film Preparation	33
Experimental Procedure	34
Adenine	34

CHAPTER	PAGE
Cytosine, thymine, and uracil	42
V. RESULTS AND DISCUSSION	46
Adenine	46
Cytosine, Thymine, and Uracil	60
VI. SUMMARY	64
BIBLIOGRAPHY	66
VITA	70

LIST OF FIGURES

FIGURE		PAGE
1.	Molecular structure of the nucleic acid bases	2
2.	Structure of DNA	4
3.	Schematic diagram of a planar thin film of thickness d and infinite area bounded on either side by semi-infinite media	13
4.	Behavior of the real and imaginary parts of the dielectric constant and the energy loss function for a) Drude's ($\hbar\omega_p$ = 20 eV and $\hbar\gamma$ = 2 eV) and b) Lorentz's model ($\hbar\omega_p$ = 20 eV, $\hbar\omega_o$ = 10 eV, and $\hbar\gamma$ = 2 eV)	25
5.	Schematic diagram, top view, of the grazing incidence monochromator and experimental chamber	31
6.	The real and imaginary parts n and k of the refractive index of adenine as a function of incident photon energy	36
7.	Near-normal incidence reflectance of adenine films as a function of incident photon energy	38
8.	The real and imaginary parts n and k of the refractive index of adenine as a function of incident photon energy	39

FIGURE PAGE

9. Contribution to the phase change on reflection due to absorption in the energy region above 82 eV for adenine as a function of incident photon energy 41

10. The real and imaginary parts n and k of the refractive index of cytosine as a function of incident photon energy 43

11. The real and imaginary parts n and k of the refractive index of thymine as a function of incident photon energy 44

12. The real and imaginary parts n and k of the refractive index of uracil as a function of incident photon energy 45

13. The extinction coefficient, k, of adenine as a function of incident photon energy compared with the values obtained by Tang et al. (1973) from transmission measurements 47

14. The real and imaginary parts ϵ_1 and ϵ_2 of the complex dielectric constant ϵ of adenine as a function of incident photon energy 50

15. Energy loss function, $-\mathrm{Im}(1/\epsilon)$, of adenine as a function of incident photon energy 51

FIGURE PAGE

16. The effective number of electrons participating in optical excitations $[n_{eff}(\epsilon_2)]$ and the effective number of electrons participating in energy losses $[n_{eff}(\mathrm{Im}(1/\epsilon))]$ in adenine up to an incident photon energy E_o 59

17. The real and imaginary parts ϵ_1 and ϵ_2 of the complex dielectric constant ϵ and the energy loss function, $-\mathrm{Im}(1/\epsilon)$, of cytosine as a function of incident photon energy 61

18. The real and imaginary parts ϵ_1 and ϵ_2 of the complex dielectric constant ϵ and the energy loss function, $-\mathrm{Im}(1/\epsilon)$, of thymine as a function of incident photon energy 62

19. The real and imaginary parts ϵ_1 and ϵ_2 of the complex dielectric constant ϵ and the energy loss function, $-\mathrm{Im}(1/\epsilon)$, of uracil as a function of incident photon energy 63

CHAPTER I

INTRODUCTION

I. INTRODUCTION

For a proper understanding of the problems associated with radiation damage to living material, it is essential to determine the basic electronic properties of the important biological molecules. The nucleic acids are very minor constituents of living matter from a quantitative viewpoint, but, because they control the processes of heredity by which cells and organisms reproduce their proteins and themselves, they are extremely important. If anything may be said to be the key to the distinction between living and non-living matter, it is the nucleic acids. Nucleic acid molecules consist of long chains of units called nucleotides. Both the kinds of nucleotide present and their arrangement govern the biological behavior of a nucleic acid. Each nucleotide has three parts, a phosphate group (PO_4), a pentose sugar, and a nitrogen base. A pentose sugar is one that contains five carbon atoms. In ribonucleic acid (RNA) the sugar is ribose, $C_5H_{10}O_5$, and in deoxyribonucleic acid (DNA) the sugar is deoxyribose, $C_5H_{10}O_4$, which has one 0 atom less than ribose. The five nitrogen bases usually found in nucleic acids are adenine, guanine, and cytosine, which occur in both RNA and DNA, and thymine and uracil, which occur respectively in DNA and RNA only. The structures of these nitrogen bases are given in Figure 1.

A DNA molecule is composed of two chains of nucleotides spiraling around a common center to form a double helix. The DNA structure is shown

ORNL-DWG. 73-5001

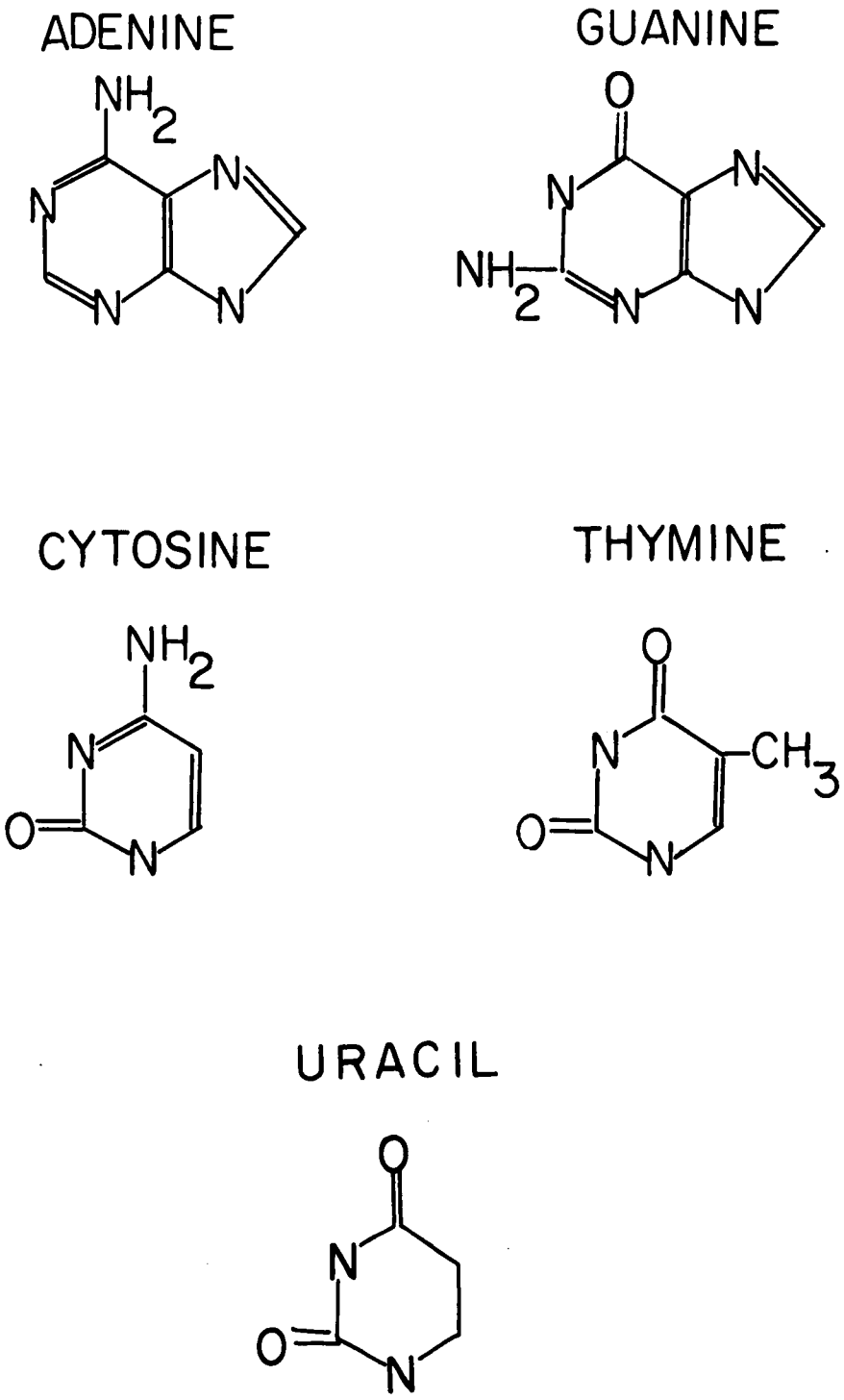

Figure 1. Molecular structure of the nucleic acid bases.

in Figure 2. The bases of one chain are bonded by hydrogen bonds to the bases of the other chain. These bonds are formed only between specific pairs of bases. Adenine, in one chain, is always bonded to thymine in the other chain and cytosine is always bonded to guanine. Because the bases will pair in only one way, the sequence of bases in one chain determines the sequence of bases in the other. The genetic information is determined by the various sequences. This model of DNA was proposed by Watson and Crick (1953). The other type of nucleic acid, RNA, differs from DNA in a number of respects. RNA molecules are much smaller than DNA molecules, for example, and usually consist of only single strands of nucleotides. Furthermore, as mentioned earlier, ribose instead of deoxyribose sugar is incorporated in each RNA nucleotide, and uracil replaces thymine as one of the pyrimidine bases.

II. REVIEW OF PREVIOUS WORK

One of the most direct methods of obtaining the basic electronic properties of a material is to determine optically the real and imaginary parts n and k, respectively, of the complex refractive index $\tilde{n} = n + ik$. However until recently such direct optical measurements on biological materials have been very limited. Absorption spectra of the nucleic acid bases have been obtained from transmission measurements for the vapor, solution, and solid states up to a maximum photon energy of 10 eV (shown in Table I for adenine). These measurements yield quantities proportional to

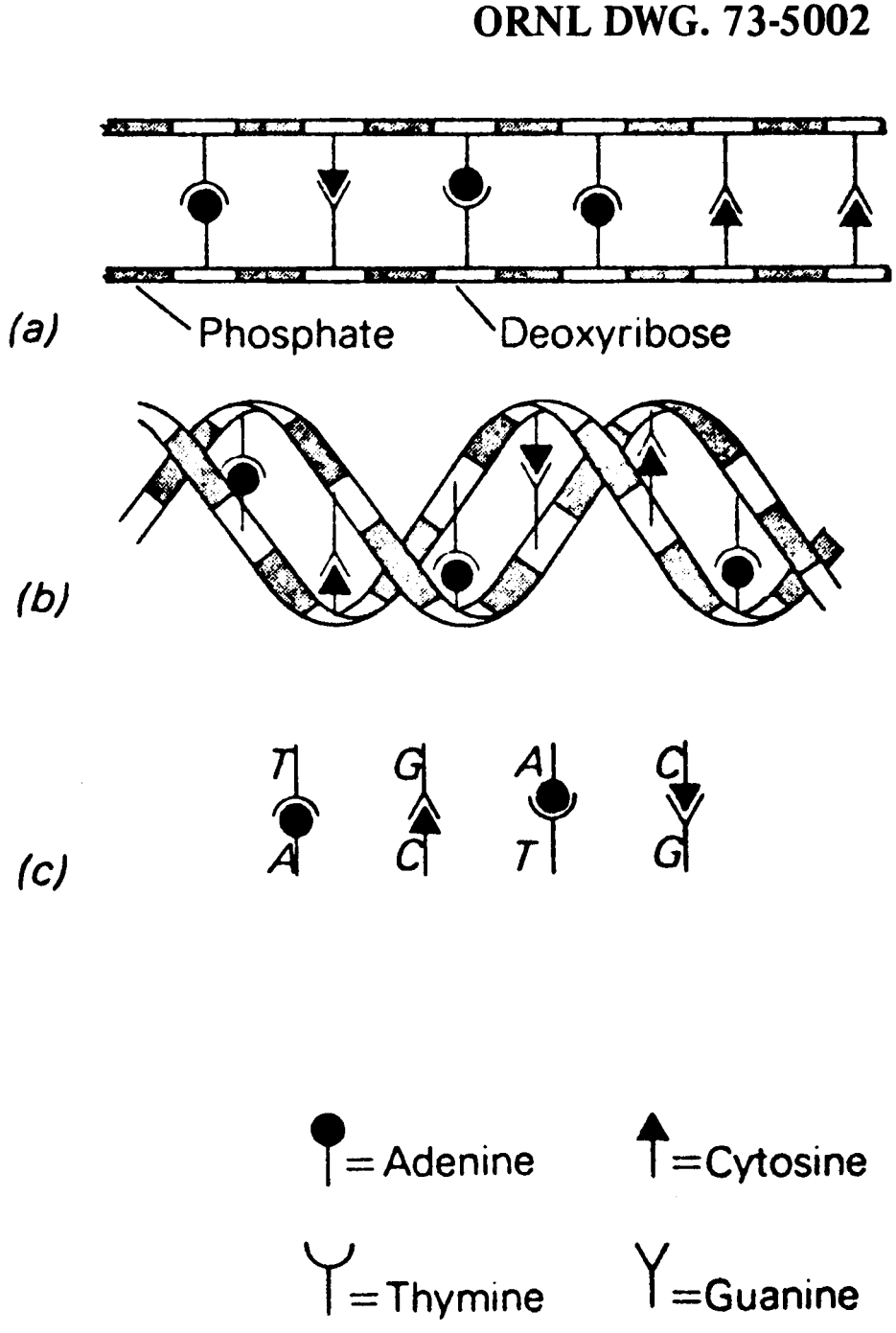

Figure 2. Structure of DNA

a) Nitrogen bases link alternate phosphate and deoxyribose groups. b) The double helix. c) The pairing of the bases.

TABLE I

REVIEW OF PREVIOUS OBSERVATIONS OF ABSORPTION SPECTRA OF ADENINE

Author	Form	Range of Measurements (eV)	Absorption Peaks (eV)	Comments
Sinsheimer et al. (1950)	Solid	4-5.1	Broad peak at 4.6	Measurements taken immediately and on a three day old film show signs of aging
Preiss and Setlow (1956)	Solution	5.1-6.0		
Voet et al. (1963)	Solution	4-6.8	4.72 6.18 4.76 5.99	In water pH 2.5 In water pH 7.0
Clark et al. (1965)	Vapor	4-6.2	4.92 5.99	
Tanaka and Nagakura (1966)	Solid	4.28-7.75	4.43, 4.59, 5.88, 6.63, 7.65	Evaporated on quartz
	Solution	4.4-7.0	4.77, 6.05, 6.85	In water
Kleinwachter et al. (1967)	Solution	4-5.5	4.56, 4.64, 4.71, 4.79 4.46, 4.63, 4.82	Isopropanol at 150°K Acetate pH 7.0 at room temperature
Yamada and Fukutome (1968)	Solid	3-10	4.59, 5.90, 6.80, 7.74	Sublimed on LiF

TABLE I (continued)

Author	Form	Range of Measurements (eV)	Absorption Peaks (eV)	Comments
Onari and Watanabe (1970)	Solid	4-10	4.85, 6.0, 6.6, 7.85	Compared with poly A and ribose phosphate
Tang et al. (1973)	Solid	4-10	4.50, 5.81, 6.74, 7.80, 8.75	Transmission and reflectance gave n and k

the imaginary part, k, of the refractive index. Tang et al. (1973) also obtained the real part, n, of the refractive index. Experimental work on the conductivity and dielectric constants of DNA and related compounds have been done by Weissbluth (1971), O'Konski et al. (1970), Snart (1968), and Inagaki et al. (1974). Theoretical calculations of the spectral properties of DNA have been carried out by Rhodes (1961), Ladik (1971), Pullman and Pullman (1969), Fenton (1965) and Hoffman and Ladik (1964). There is still no completely satisfactory electronic structure model for DNA.

Electron energy loss measurements for the bases using a scanning electron microscope equipped with a high resolution magnetic spectrometer have been reported by Johnson (1972) and Isaacson (1972). Electron energy loss spectra up to $\sim$ 500 eV have been obtained for $\sim$ 25 keV electrons incident on solid films of the individual nucleic acid bases. These measurements give directly the energy losses suffered by the incident electrons but do not identify the type of excitations which are produced in the irradiated material. Optical properties are frequently calculated from electron energy loss spectra. However, these calculations involve a number of theoretical assumptions, and significant discrepancies can exist between data obtained by electron energy loss studies and by direct optical studies. Eventually the aim is to refine the scanning electron microscope measurements so that the sequence of bases in a particular DNA molecule can be identified from the spectra of the individual bases. It has been thought that the results might be affected by radiation damage done to the DNA molecule by the scanning electron beam. As a

check on this, a study of the optical properties of the nucleic acid bases was initiated by Tang et al. (1973). This study, which is continued in this investigation, enables us to calculate energy loss functions which can be compared with those calculated from the measured electron energy loss spectra.

III. PRESENT WORK

The present work is an extension of the work of Tang et al. (1973). We have determined the optical properties n and k from reflection measurements for solid films of adenine over the range of photon energies from 4 to 82 eV. The values for n and k were used to calculate the complex dielectric constant $\epsilon = \epsilon_1 + i\epsilon_2$, where $\epsilon_1 = n^2 - k^2$ and $\epsilon_2 = 2nk$, and the electron energy loss function = $-\mathrm{Im}(1/\epsilon)$. These optical properties have been analyzed in terms of $\pi \rightarrow \pi^*$ and $\sigma \rightarrow \sigma^*$ molecular excitations and of collective excitations in the solid of the loosely bound electrons. The electron energy loss function, $-\mathrm{Im}(1/\epsilon)$, as a function of incident photon energy, calculated from our optical properties has been compared with the values calculated from the electron energy loss spectrum for adenine obtained by Isaacson (1972). Possible reasons for differences in the two spectra are discussed.

Measurements of reflectance as a function of photon angle of incidence have also been obtained for cytosine, thymine, and uracil over the range of photon energies from 25 to 82 eV, and analyzed to give n, k, ϵ_1, ϵ_2, and $-\mathrm{Im}(1/\epsilon)$ over this energy range for these materials. Whereas for adenine our data below 10 eV are compared with previously published data, our optical

data above 10 eV are presented for the first time for the four materials, adenine, cytosine, thymine and uracil.

CHAPTER II

THEORY

I. OPTICAL CONSTANTS

When electromagnetic radiation is incident on a boundary separating two different media, part of it is reflected, and part of it is transmitted into the second medium. The amount of radiation that is reflected or transmitted is determined by the optical properties of the medium. The optical properties can be characterized by the optical constants, n and k, the real and imaginary parts, respectively, of the complex index of refraction, $\tilde{n}$, where n, the index of refraction, is defined as the ratio of the velocity of the radiation in vacuum to its phase velocity in the medium, $n = c/v$, and k is often referred to as the extinction coefficient.

For a plane electromagnetic wave traveling in the positive z direction in an absorbing medium the equations for the amplitudes of the electric and magnetic fields can be written as

$$\vec{E} = \vec{E}_o \exp\left[i\left(\frac{2\pi n}{\lambda} z - \omega t\right)\right] \exp\left[-\frac{2\pi k}{\lambda} z\right] \tag{1}$$

$$\vec{H} = \vec{H}_o \exp\left[i\left(\frac{2\pi n}{\lambda} z - \omega t\right)\right] \exp\left[-\frac{2\pi k}{\lambda} z\right] \tag{2}$$

where z is the distance and t is the time of propagation of the wave through the medium, $\vec{E}_o$ and $\vec{H}_o$ are the electric and magnetic field intensities at

$z = 0$ and $t = 0$, ω is the frequency, and λ is the wavelength in vacuum. The problem of determining the amount of light reflected and transmitted by an optical system may be solved by using Maxwell's equations with suitable boundary conditions. For an isotropic medium with zero charge density and negligible magnetic susceptibility, Maxwell's equations can be written

$$\nabla \cdot \vec{E} = 0 \ , \tag{3}$$

$$\nabla \cdot \vec{H} = 0 \ , \tag{4}$$

$$\nabla \times \vec{E} = -\frac{1}{c}\frac{\partial \vec{H}}{\partial t} \ , \tag{5}$$

$$\nabla \times \vec{H} = \frac{\epsilon}{c}\frac{\partial \vec{E}}{\partial t} \ . \tag{6}$$

The dielectric constant, ϵ, is a complex quantity with real and imaginary parts ϵ_1 and ϵ_2, respectively. Equation (5) can be solved for $\vec{E}$ by taking the curl of Equation (5) and substituting for $\nabla \times \vec{H}$ from Equation (6) giving

$$\nabla^2 \vec{E} = \frac{\epsilon}{c^2}\frac{\partial^2 \vec{E}}{\partial t^2} \tag{7}$$

and similarly for the magnetic vector

$$\nabla^2 \vec{H} = \frac{\epsilon}{c^2}\frac{\partial^2 \vec{H}}{\partial t^2} \ . \tag{8}$$

Substituting Equation (1) into Equation (7) shows that

$$\epsilon = \tilde{n}^2 \tag{9}$$

so that the dielectric constants, ϵ_1 and ϵ_2, are related to the optical constants, n and k, by

$$\epsilon_1 = n^2 - k^2 \tag{10}$$

$$\epsilon_2 = 2nk \ . \tag{11}$$

Hence the measurements of n and k give ϵ_1 and ϵ_2. Both ϵ and $\tilde{n}$ contain the same physical information.

Reflectance

Consider a planar thin film of thickness d and infinite area bounded on either side by semi-infinite non-absorbing media as shown in Figure 3. Let medium 0 have index of refraction n_o, and the semi-infinite substrate described by medium 2 have index of refraction n_2. Both media 0 and 2 are transparent, i.e., $k_o = 0$ and $k_2 = 0$. The thin film is described by medium 1 with optical constants n_1 and k_1. Let the light be incident through medium 0 at an angle of incidence ϕ_o with respect to the normal to the interface between media 0 and 1. Since the incident light is partially polarized, both components must be treated. Let subscript s denote the electric vector perpendicular to the plane of incidence and p denote the electric vector parallel to the plane of incidence. Then the amplitudes of the reflected and transmitted components are

$$r_{1p} = \frac{\sigma_1 - \epsilon_1 \mu}{\sigma_1 + \epsilon_1 \mu} \tag{12}$$

$$r_{2p} = \frac{\epsilon_1 \sigma_2 - \epsilon_2 \sigma_1}{\epsilon_1 \sigma_2 + \epsilon_2 \sigma_1} \tag{13}$$

ORNL-DWG. 73-5003

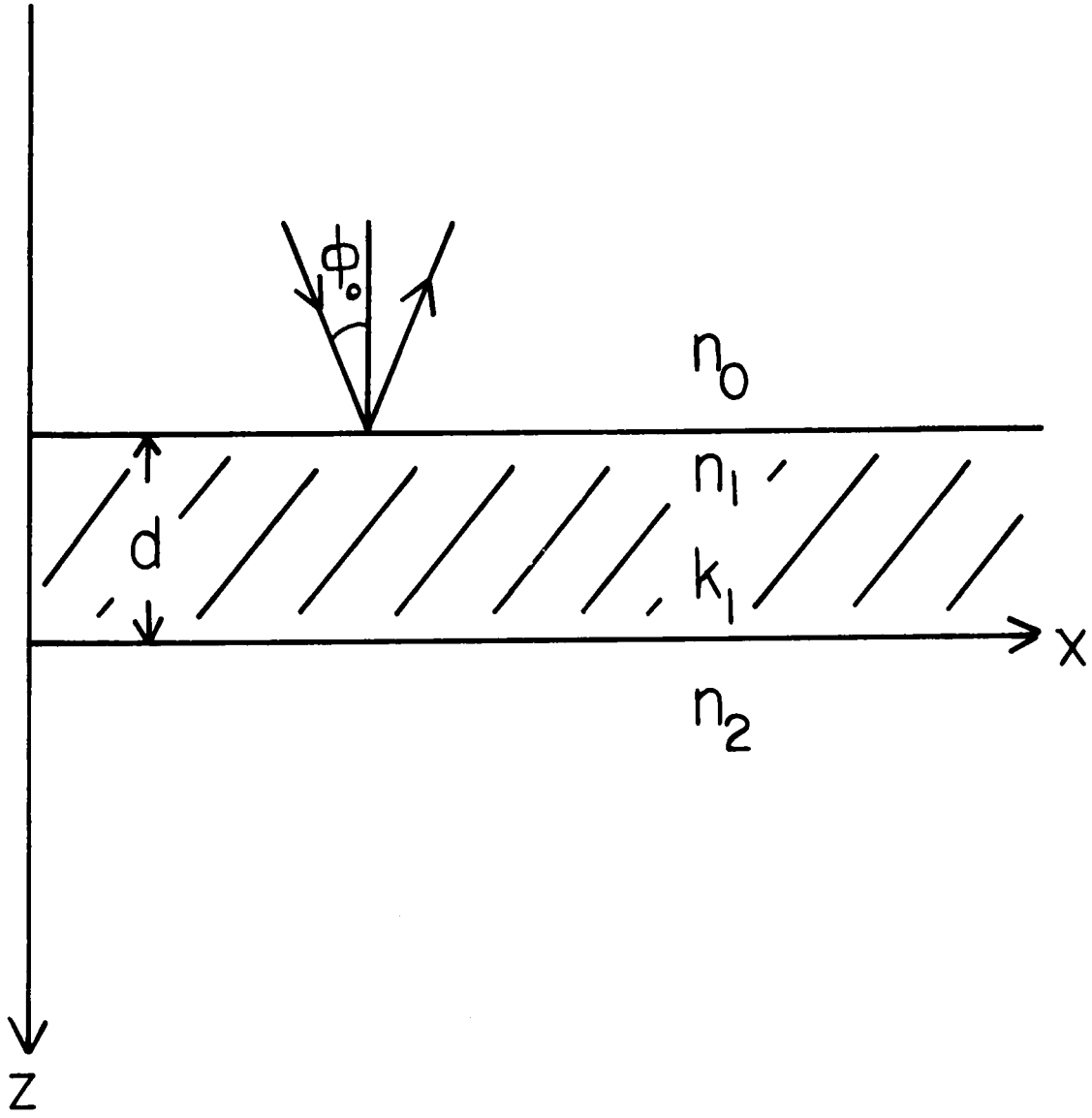

Figure 3. Schematic diagram of a planar thin film of thickness d and infinite area bounded on either side by semi-infinite media.

$$t_{1p} = \frac{2\mu\tilde{n}_1}{\sigma_1 + \epsilon_1\mu} \tag{14}$$

$$t_{1p}' = \frac{2\sigma_1\tilde{n}_1}{\sigma_1 + \epsilon_1\mu} \tag{15}$$

$$r_{1s} = \frac{\mu - \sigma_1}{\mu + \sigma_1} \tag{16}$$

$$r_{2s} = \frac{\sigma_1 - \sigma_2}{\sigma_1 + \sigma_2} \tag{17}$$

$$t_{1s} = \frac{2\mu}{\mu + \sigma_1} \tag{18}$$

$$t_{1s}' = \frac{\sigma_1}{\mu + \sigma_1} \tag{19}$$

where r_{1p} and r_{1s} are the amplitudes of the parallel and perpendicularly polarized light reflected from the interface between media 0 and 1, respectively, r_{2p} and r_{2s} are the amplitudes of the parallel and perpendicularly polarized light reflected from the interface between media 1 and 2, respectively, t_{1p} and t_{1s} are the amplitudes of the parallel and perpendicularly polarized light transmitted from medium 0 to medium 1, respectively and t_{1p}', and t_{1s}', are the amplitudes of the parallel and perpendicularly polarized light transmitted from medium 1 to 0 after it is reflected from

the interface between media 1 and 2, respectively. $\tilde{n}_1$, $\tilde{n}_2$, ϵ_1, ϵ_2, σ_1, σ_2, μ, and δ are defined as

$$\tilde{n}_1 = \frac{n_1 + ik_1}{n_o} \tag{20}$$

$$\tilde{n}_2 = \frac{n_2}{n_o} \tag{21}$$

$$\epsilon_1 = \tilde{n}_1^2 \tag{22}$$

$$\epsilon_2 = \tilde{n}_2^2 \tag{23}$$

$$\sigma_1 = \sqrt{\epsilon_1 - \sin^2\phi_o} \tag{24}$$

$$\sigma_2 = \sqrt{\epsilon_2 - \sin^2\phi_o} \tag{25}$$

$$\mu = \cos\phi_o \tag{26}$$

and

$$\delta = \frac{2\pi d}{\lambda} n_o \sigma_1 \quad . \tag{27}$$

Then the amplitude of the light reflected by this system is given by

$$r_i = r_{1i} + \frac{t_{1i} t_{1i}' r_{2i} e^{2i\delta}}{1 + r_{1i} r_{2i} e^{2i\delta}} \tag{28}$$

where i = p, s. The reflectance of this system is given by

$$R = \frac{|r_s|^2 + P|r_p|^2}{1 + P} \tag{29}$$

where

$$P = \frac{I_p}{I_s} \tag{30}$$

is the ratio of the light intensity polarized parallel to the plane of incidence to that polarized perpendicular to the plane of incidence.

In this investigation the value of P was known for each incident photon energy. Equation (29) was then used in two ways. First, in the transparent region where k = 0, interference affects the normal incidence reflectance, R_n. In this energy region a plot of R_n vs. incident photon energy was analyzed to yield the film thickness and n vs. incident photon energy. Secondly, for $h\nu > 33$ eV where R_n is small and a direct measurement is associated with a large percentage uncertainty, the reflectance was measured as a function of angle of incidence, ϕ, from 50° to 86°. For these measurements the film thickness was effectively infinite and a least squares fit of $R(\phi)$, vs. ϕ to Equation (29) for a given photon energy yielded values of n and k at that energy. The various factors influencing the accuracy with which n and k ($k \neq 0$) can be determined by this method have been discussed by Hunter (1965). Thirdly, in the intermediate energy region where R_n is sufficiently large that a direct measurement is possible, and where the R vs. ϕ method is insensitive, values of n and k were obtained from a Kramers-Kronig analysis.

Kramers-Kronig Analysis of the Reflectance Data

At normal incidence the measured reflectance is no longer a function of the polarization of the incident radiation, and Equation (29) reduces to a simple expression for R in terms of n and k,

$$R_n = R = \left| \frac{\tilde{n} - 1}{\tilde{n} + 1} \right|^2 = \frac{(n-1)^2 + k^2}{(n+1)^2 + k^2} \quad . \tag{31}$$

If we define a complex reflection amplitude $\sqrt{\tilde{R}}$ by the equation,

$$\sqrt{\tilde{R}} = \sqrt{R}\, e^{i\theta} \quad , \tag{32}$$

and separating the real and imaginary parts of Equation (32), the following expressions are obtained for n and k;

$$n = \frac{1 - R}{1 + R - 2\sqrt{R}\cos\theta} \quad ,$$

and

$$k = \frac{-2\sqrt{R}\sin\theta}{1 + R - 2\sqrt{R}\cos\theta} \quad . \tag{33}$$

$\tilde{R}$ is a complex, analytic function of the photon energy E, and the dispersion relation between the real and imaginary parts may be written in the form [Bode (1945)] ,

$$\theta(E) = \frac{\mathcal{P}}{\pi} \int_0^\infty \ln \left| \frac{E'-E}{E'+E} \right| \frac{d \ln \sqrt{R(E')}}{dE'} \, dE' \quad , \tag{34}$$

where $\theta(E)$ is the phase change on reflection at the energy E, and $\mathcal{P}$ denotes the Cauchy principal value. Thus, if the normal incidence reflectance is known over the spectral region of photon energies from zero to infinity, $\theta(E)$ is determined by Equation (34) and the optical constants are calculated using Equations (33).

The requirement that the reflectance be known for all energies is impossible to satisfy, so the problem of obtaining the contribution to the integral from the spectral regions beyond the limits of experimental measurements must be solved. For an insulating material, such as adenine, measurements of n and hence R_n [from Equation (31)] in the transparent (k = 0) region can be extrapolated with little uncertainty down to E = 0. The high energy region presents a more complicated situation because there is no way of predicting exactly how R_n will behave above the highest energy data point and, furthermore, the contribution to the integral is expected to be significant. The slope of the energy dependent reflectance may be large enough to offset the decreasing logarithmic term in the integrand of Equation (34). If the high energy region is void of interband effects, however, the reflectance is expected to fall off as E^{-4}, showing, at high enough energies, metallic-like behavior.

In the presence of interband effects, suitable extrapolation procedures are not immediately obvious, but a method suggested by MacRae, Arakawa, and Williams (1967) provides a relatively simple means of evaluating the

contribution to $\theta(E)$ from the integration over energies extending from the last experimental point to infinity. Integration of the Kramers-Kronig integral by parts yields the following result:

$$\theta(E) = \frac{E}{\pi} \mathcal{P} \int_0^\infty \frac{\ln R(E')}{(E')^2 - E^2} \, dE' \quad ,$$

or

$$\theta(E) = \frac{E}{\pi} \mathcal{P} \int_0^{E_c} \frac{\ln R(E')}{(E')^2 - E^2} \, dE' + \frac{E}{\pi} \mathcal{P} \int_{E_c}^\infty \frac{\ln R(E')}{(E')^2 - E^2} \, dE' \quad . \tag{35}$$

Thus, the phase change on reflection may be written as the sum of contributions from the experimental region, from zero to the cutoff energy E_c, and the extrapolated region, from E_c to infinity;

$$\theta(E) = \theta_{KK}(E) + \Delta\theta(E) \quad . \tag{36}$$

θ_{KK} is the first term in Equation (35), and the integral is evaluated numerically. $\Delta\theta(E)$ is the second term in Equation (35), and independent measurements of n and k at selected energies in the experimental region are used to establish the form of $\Delta\theta(E)$ over the entire experimental region. By eliminating R from the equations for n and k [Equations (33)] it is possible to derive the relationship,

$$\theta(E) = \tan^{-1}\left[\frac{2k}{1-n^2-k^2}\right] ; \qquad (37)$$

so, if n and k are known at an energy E_o, $\Delta\theta(E_o)$ is determined directly from Equation (36). It is then possible to interpolate between values of $\Delta\theta(E_o)$ plotted as a function of E_o to determine the contribution to $\theta(E)$ from the extrapolated region at all energies E in the experimental region. The function $\Delta\theta(E_o)$ is not expected to show structure because any rapid variation in $R(E')$ are subsequently smeared out by the integration over all energies from E_c to infinity. In fact, $\Delta\theta(E)$ must be a smoothly varying monotonic function of E with $d(\Delta\theta)/dE \leq 0$ and $d^2(\Delta\theta)/dE^2 \leq 0$. The exact form of $\Delta\theta(E)$ depends on the 'correct' extrapolation of R_n above E_c, which of course if not known. The only additional restriction put on $\Delta\theta(E)$ when, as in the present case, reflectance measurements are extended well above the energies of the molecular excitations is that the sum rules (see below) over $\epsilon_2 E$ and over $-\mathrm{Im}\,(1/\epsilon)\cdot E$ should saturate by E_c at the same number of electrons.

Sum Rules

The sum rules

$$n_{eff}[\epsilon_2, E_o] = \frac{m}{2\hbar^2\pi^2 e^2 N}\int_o^{E_o} \epsilon_2 \cdot E\, dE \qquad (38)$$

and

$$n_{eff}[-Im(\epsilon)^{-1}, E_o] = \frac{m}{2\hbar^2 \pi^2 e^2 N} \int_o^{E_o} -Im(\epsilon)^{-1} \cdot E \, dE \qquad (39)$$

are used to calculate, respectively, the effective number of electrons per molecule contributing to optical transitions and to the electron energy loss up to an energy E_o. Here m and e are the electron mass and charge and N is the molecular density.

Energy Loss Function

The probability that a fast, charged particle traversing a solid will lose an amount of energy equal to $\hbar\omega$ was shown by Ritchie (1957) to be related to the function $-Im(1/\epsilon)$. In terms of the real and imaginary parts of the dielectric constant of the medium, this energy loss function is

$$-Im(1/\epsilon) = \frac{\epsilon_2}{\epsilon_1^2 + \epsilon_2^2} \quad . \qquad (40)$$

Thus if the optical and dielectric constants are obtained for a medium from measurements of reflectance, the energy loss function can be calculated from Equation (40). This can be compared with electron energy loss measurements for the same material.

II. CLASSICAL DIELECTRIC THEORY

The distinction between metals and insulators is frequently based upon their responses to the dc electric field. However, the optical properties of metals and insulators have much in common in the ultraviolet. The model that the electrons in a metal form a gas of free particles was proposed by Drude. An equally simple picture for insulators was proposed by Lorentz. In this case the electrons can be envisioned as tied to certain equilibrium positions by springs.

The response of one of the electrons of mass m and charge -e, in a Lorentz insulator to a uniform oscillating electric field, $\vec{E} = \vec{E}_o e^{-i\omega t}$, is described by the equation of motion

$$\frac{d^2\vec{X}}{dt^2} + \gamma \frac{d\vec{X}}{dt} + \omega_o^2 \vec{X} = \frac{-e\vec{E}}{m} \quad . \tag{41}$$

Here $\gamma \frac{d\vec{X}}{dt}$ is the damping term proportional to the velocity and characterized by a damping constant γ, ω_o is the natural frequency associated with Hooke's Law describing the restoring force of a spring, and the right hand side of the equation represents the driving term due to the electric field.

Since the equation is linear in the displacement X, we may assume that it has the same time dependence as $\vec{E}$. Then the displacement is

$$\vec{X} = \frac{-e\vec{E}}{m(\omega_o^2 - \omega^2 - i\gamma\omega)} \quad . \tag{42}$$

For a dielectric material with N electrons per unit volume the polarization is defined as

$$\vec{P} = -Ne\vec{X} \tag{43}$$

and is related to the electric field by

$$\vec{P} = \frac{(\epsilon - 1)}{4\pi}\vec{E} \quad . \tag{44}$$

Thus from Equations (42) and (43) the polarization can be written as

$$\vec{P} = \frac{Ne^2\vec{E}}{m(\omega_o^2 - \omega^2 - i\gamma\omega)} \quad . \tag{45}$$

Substitution of Equation (45) into Equation (44) yields

$$\epsilon = 1 + \frac{4\pi Ne^2/m}{(\omega_o^2 - \omega^2 - i\gamma\omega)} \quad . \tag{46}$$

The real and imaginary parts of the dielectric constant, ϵ_1 and ϵ_2, can be written respectively as

$$\epsilon_1 = 1 + \left(\frac{4\pi Ne^2}{m}\right)\left(\frac{(\omega_o^2 - \omega^2)}{(\omega_o^2 - \omega^2)^2 + \gamma^2\omega^2}\right) \tag{47}$$

$$\epsilon_2 = \left(\frac{4\pi Ne^2}{m}\right)\left(\frac{\gamma\omega}{(\omega_o^2 - \omega^2)^2 + \gamma^2\omega^2}\right) \quad . \tag{48}$$

The behavior for the real and imaginary parts of the dielectric constants for both Lorentz's and Drude's models are shown in Figure 4, and it is seen that at sufficiently high energies the dielectric response is very similar in metals and insulators. The energy loss function [$-\mathrm{Im}(1/\epsilon)$] calculated for the given values of ϵ_1 and ϵ_2 are also shown. The dissipation of electromagnetic energy in the medium is given by [Kloos (1968)]

$$\frac{dW}{dt} = \epsilon_2 \omega \vec{E}^2 \tag{49}$$

where $\vec{E}$ is the electric field of the photon. Thus, ϵ_2 should show structure where certain excitations of electrons occur with high probability, and the theoretical band structure can be checked by comparing it with the spectral dependence of ϵ_2.

The condition for the existence of collective oscillations is that the complex dielectric constant $\epsilon = 0$. In practice, it is not necessary to require that $\epsilon_1 = 0$ in the region where $\epsilon = 0$. It has been shown that the maximum of $-\mathrm{Im}(1/\epsilon)$ corresponds to a collective resonance if ϵ_1 and ϵ_2 are (i) small in the region of the peak, (ii) approximately linearly varying with $d\epsilon_1/d\omega > 0$ and $d\epsilon_2/d\omega < 0$ and (iii) $(\omega/\epsilon_1)\, d\epsilon_1/d\omega$ and $(\omega/\epsilon_2)\, d\epsilon_2/d\omega \gg 1$ [Ehrenreich and Phillipp (1962)]. It is shown by Powell (1969) that it is difficult in metals to correlate maxima in $-\mathrm{Im}\,(1/\epsilon)$ with maxima in ϵ_2 and to identify a particular maximum in $-\mathrm{Im}(1/\epsilon)$ as being associated with a volume plasmon excitation. Maxima in $-\mathrm{Im}(1/\epsilon)$ may occur at substantially different frequencies and with differing relative intensities than maxima in ϵ_2. Williams et al. (1974) have

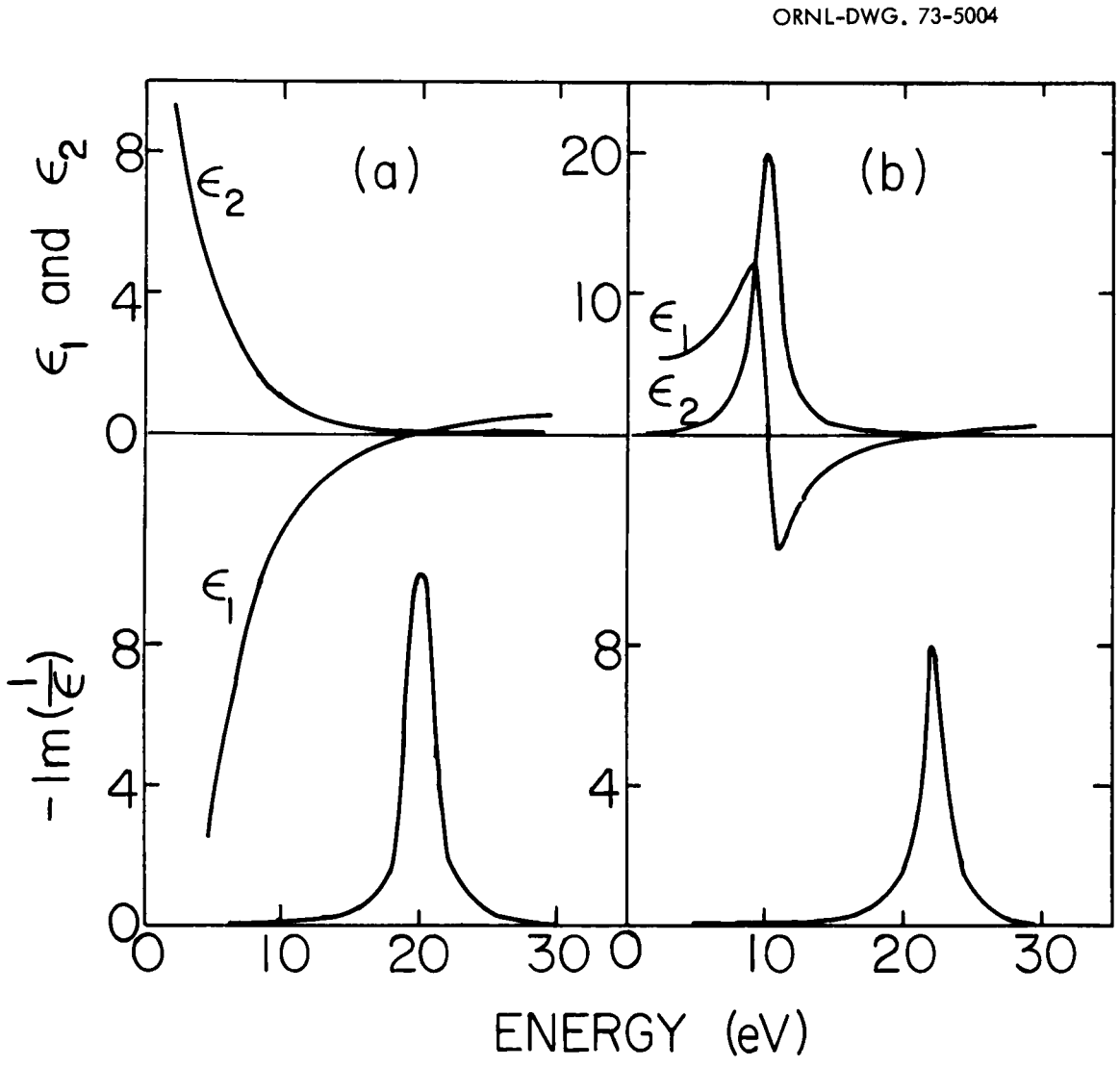

Figure 4. Behavior of the real and imaginary parts of the dielectric constant and the energy loss function for a) Drude's ($\hbar\omega_p$ = 20 eV and $\hbar\gamma$ = 2 eV) and b) Lorentz's model ($\hbar\omega_p$ = 20 eV, $\hbar\omega_o$ = 10 eV, and $\hbar\gamma$ = 2 eV).

made similar observations for molecular liquids, concluding that for each maximum in ϵ_2 there is a corresponding, single, maximum in $-\mathrm{Im}(1/\epsilon)$, and that the separation in energy in those two maxima indicates the degree of collective behavior exhibited by the loosely bound electrons in the system.

III. COVALENT BONDING

In order to interpret the structure of the organic compounds from the optical data, a brief description of the molecular orbital picture and covalent bonding is given in this section.

Atoms are held together in a molecule by chemical bonds. There are usually two kinds of bonding in molecules, the ionic bond and the covalent bond. The ionic bond results from the transfer of electrons, while the covalent bond results from sharing of electrons. Covalent bonding is the more important in organic molecules.

A carbon atom forms four covalent bonds with other atoms by promoting one of its 2s electrons to the vacant 2p orbital and the four orbitals hybridize to form four sp^3 orbitals. In some molecules with a carbon-carbon bond three hybrid sp^2 orbitals form bonds with three other atoms such as hydrogen. These sp^2 orbitals lie in one plane and form bonds which are cylindrically symmetrical about a line joining the nuclei. These are called σ bonds. The remaining p orbital consists of two equal lobes, one lying above and the other lying below the plane of the three sp^2 orbitals, and is occupied by a single electron. If this p orbital of one carbon atom overlaps the p orbital of another carbon atom,

the electrons pair up and an additional bond, called a π-bond, is formed. The π-bond thus consists of two parts, one electron cloud lies above the plane of the atoms and another electron cloud lies below. π-bonds are weaker than σ-bonds because of less overlapping. Similarly in a benzene ring, three sp^2 orbitals are used for each carbon atom to form a hexagon. All the atoms of benzene lie in one plane. Hence as before, these bonds are σ bonds. The remaining p orbital of each carbon atom overlaps the p orbital of an adjacent carbon atom, and a π-bond is formed. But the overlapping is not limited to a pair of p orbitals. The p orbital of any one carbon atom overlaps equally well the p orbitals of both carbon atoms to which it is bonded. The result is two continuous doughnut-shaped electron clouds, one lying above and one lying below the plane of the C_6H_6 molecule. Overlapping of atomic orbitals can also result in an electron density between the atomic nuclei which is less than that at the same distance from the nucleus in an isolated atom. These states are called antibonding and are designated as σ^* and π^*. They are less stable than the corresponding bonding states and hence have higher energies. There are unshared electrons or non-bonded electrons in molecules containing atoms like nitrogen, oxygen, etc. They are usually called n-electrons and are less tightly bound to the molecule than the σ and π electrons. In general the $n \rightarrow \pi^*$ transitions require the smallest energy followed by $n \rightarrow \sigma^*$, $\pi \rightarrow \pi^*$, and $\sigma \rightarrow \sigma^*$ in that order. The $n \rightarrow \pi^*$ and $n \rightarrow \sigma^*$ transitions are usually found in the visible through the near ultraviolet. The $\pi \rightarrow \pi^*$ transitions are observed in the ultraviolet through the vacuum ultraviolet and the $\sigma \rightarrow \sigma^*$ transitions only in the vacuum ultraviolet.

The above picture provides only a qualitative description of the processes involved in molecular bonding for organic compounds. For a particular molecule and its energy transitions, detailed calculations must be used to account for all the processes of molecular bonding.

CHAPTER III

EXPERIMENTAL APPARATUS

The experiment involves two pieces of apparatus. One is for the evaporation of nucleic acid bases to make thin films on the substrate. The other is for the measurement of the optical properties of these bases. They are described separately as follows:

I. APPARATUS FOR EVAPORATION

The basic apparatus consists of a vacuum system, a coating chamber, a thickness monitor (Kronos Model QM-2), and a digital temperature indicator (Newport Series 260, Type K). The vacuum system consists of a mechanical pump, an oil diffusion pump, and a liquid nitrogen cold trap. This liquid nitrogen cold trap is used to reduce contamination due to diffusion pump oil in the high vacuum system. The nucleic acid bases were put on a flat molybdenum boat which was clamped to the electrodes which were in turn connected to a low voltage power supply. The reasons for using molybdenum as the source heater are mainly because of its low vapor pressure at high temperature and its high melting point. The thermocouple of the temperature indicator was silver soldered to the back of the boat at its center. The thickness monitor was set with the same relative geometry to the boat as the substrate in order to measure the thickness of the film.

II. APPARATUS FOR MEASURING THE OPTICAL PROPERTIES

For the range of photon energies from 2 to 18 eV a hydrogen DC discharge light source was used with a Seya-Namioka vacuum ultraviolet monochromator. This system was identical to that used by Tang et al. (1973). For the range of photon energies from 11 to 82 eV a grazing incidence monochromator (McPherson Model 247) was used. The experimental arrangement is shown schematically in Figure 5. The fixed slit and the fixed grating defined the Rowland circle and the energy (wavelength) was changed by moving the other slit along the Rowland circle. The movable slit and light source assembly was connected to the main body of the monochromator by means of a flexible stainless steel bellows which could be extended from six inches to 30 inches in length so that a large photon energy region could be scanned (10 eV < $h\nu$ < 100 eV) without breaking the vacuum. The movable slit assembly was driven by a precision screw which could be operated manually or driven by a synchronous motor and gear box. The photon spectrum could be continuously scanned at various rates from 2 inch/min. to 0.0005 inch/min. The linear dimension, inch, represents the distance from the grating to the movable slits, where for this grating and angle of incidence, a change of one inch between grating and movable slit represents a wavelength change of roughly 50 Å. The dispersing element was a concave replica diffraction grating, 2.2 meter radius with radiation from the movable slit incident on the grating. Diffracted radiation, making an angle of 82° with the grating normal, passed through the

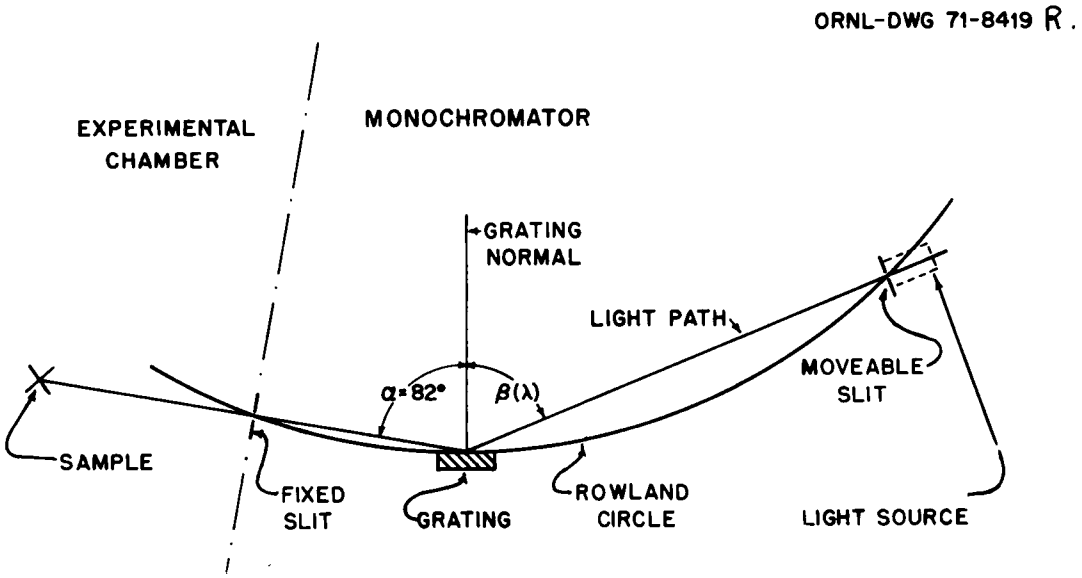

Figure 5. Schematic diagram, top view, of the grazing incidence monochromator and experimental chamber.

fixed slit into the reflectance chamber. The grating was ruled with 600 lines/mm with a blaze angle of 1°30' and overcoated with Au. Both the movable and fixed slits were continuously adjustable from 0 to 2 mm. With typical slit settings of 0.15 mm, the resolution was 1 Å. The line spectrum was produced by a high voltage pulsed discharge in air, with a pulse rate of about 20 pulses/sec. The light reflected from the specimen was detected with an open-window CuBe photomultiplier tube. The light source was operated at about 8 KV with a current of 80 ma using an air pressure of 0.08 Torr.

CHAPTER IV

EXPERIMENTAL PROCEDURE AND DETERMINATION OF OPTICAL CONSTANTS

I. SUBSTRATE CLEANING

To obtain an adherent and smooth coating on glass and other substrates, the support surface must be free from contaminant films such as grease, dirt, etc. Glass was used as a substrate throughout the experiment. Glass slides were cleaned initially with Knox-60 Laboratory Glass Cleaner, rinsed with distilled water, then put into concentrated chromic acid to remove any soap or oil films, rinsed with distilled water thoroughly, and finally flushed with isopropyl alcohol.

II. FILM PREPARATION

A thin layer of the sample which was in powdered form was put uniformly on the boat. The same molybdenum boat was used throughout the experiment. It was cleaned with water and isopropyl alcohol between evaporations. The substrates were set right above the boat at a distance of 12 cm. The thickness monitor was mounted at the same angle as the substrate with respect to the boat and at the same distance from the boat. About one hour prior to the preparation of a sample film the liquid nitrogen cold trap in the vacuum evaporator was filled. This helped to reduce the pressure of water vapor in

the chamber. Film sublimations were started when the pressure reached 6×10^{-6} Torr and then a deposition rate of approximately 500 Å/hr was maintained. The optimum sublimation temperature was for adenine,[a] 175°C; thymine,[b] 165°C; cytosine,[b] 185°C; and uracil,[c] 155°C. Because of the possibility of thermal decomposition of the nucleic acid bases, the temperatures were raised only high enough to maintain a reasonable evaporation rate. Using these methods good quality films were obtained for adenine, cytosine, and uracil. For thymine the films appeared cloudy and in order to get good quality films, it was necessary to cool the substrate with liquid nitrogen during the sublimation.

III. EXPERIMENTAL PROCEDURE

Adenine

The optical properties of adenine were determined over the energy range from 2 to 82 eV by a Kramers-Kronig analysis. If only normal or near-normal incidence reflectances R_n can be measured, this method would require that values of R_n be known from zero to infinite energy, in order to obtain

---

[a]Obtained from the Aldrich Chemical Company, Inc., Milwaukee, Wisconsin.

[b]Obtained from the Nutritional Biochemicals Corporation, Inc., Cleveland, Ohio.

[c]Obtained from the Chemical and Nuclear Corporation, Chemical and Radioisotope Division, Inc., Irvine, California.

absolute values of the optical constants n and k. In this study, R_n was obtained from 2 to 82 eV. Independent values of n and k, in selected energy regions, were also obtained. These were used for normalization purposes in the Kramers-Kronig analysis of R_n from 2 to 82 eV.

Direct measurement of R_n is difficult both at low and high energies. Below 4.2 eV adenine films are transparent and the reflectance spectrum is modified by interference. Above $\sim$ 33 eV R_n is very small and consequently difficult to measure. In the intermediate energy region the films exhibit reflectances that vary from $\sim$ 2 to 21% for which direct measurements are possible. Thus in order to obtain R_n at all energies from 2 to 82 eV it was necessary to make use of several different techniques.

At photon energies below the absorption edge in adenine the films are transparent and k = 0. From 2 to 4.2 eV the observed near-normal incidence reflectance spectrum is not characteristic of bulk adenine but is determined by interference effects in the adenine films. In this region both n as a function of incident photon energy and the film thickness, d, were obtained from an analysis of the interference structure in the reflectance spectrum measured with the Seya-Namioka monochromator. The known refractive index for the glass substrate as a function of incident photon energy was used and a 'best' fit obtained to the expression [Equation (29)] for the reflectance from a thin film. The values obtained by this method for n are shown in Figure 6, and are estimated to be accurate to $\pm$ 2%. The normal incidence reflectance R_n, characteristic of bulk adenine, was calculated from 2 to 4.2 eV by

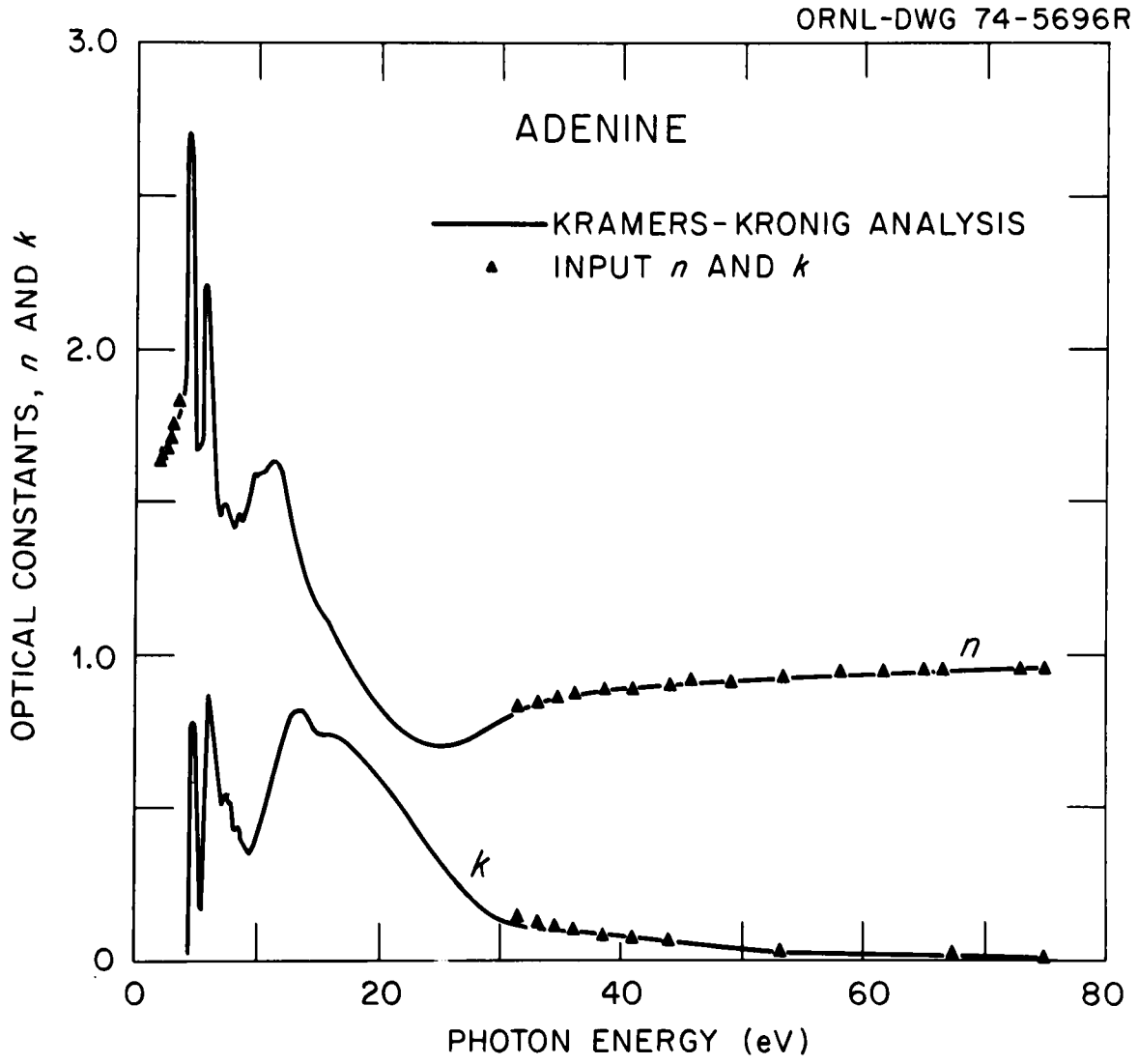

Figure 6. The real and imaginary parts n and k of the refractive index of adenine as a function of incident photon energy.

substitution of these n values and k = 0 into Equation (31). The resulting values of R_n are plotted in Figure 7.

From 4.2 to 33 eV R_n was measured directly. The Seya-Namioka monochromator was used between 4.2 and 18 eV and the grazing incidence monochromator between 11 and 33 eV. The values obtained for R_n averaged from several films are shown in Figure 7. The values are estimated to be accurate to $\pm$ 3%.

Above 33 eV, where R_n is small, reflectance as a function of angle of incidence from 50° to 86° was measured and n and k extracted at each photon energy using a two-parameter least squares fit to Fresnel's equations [Equations (29), with $d = \infty$]. The polarization, P, produced by the grating was measured as a function of photon energy using a triple-reflection polarizer [Horton et al. (1969)]. Since such a polarizer had not been calibrated in the energy region of interest here (376 → 151 Å) the instrument was first calibrated as described by Horton et al. (1969). The values obtained for n and k are shown in Figure 6, page 36. The values of n are estimated to be accurate to $\pm$ 3% and of k to $\pm$ 10%. R_n was then calculated from Equation (31), and the values obtained are plotted in Figure 7. $R(\phi)$ vs. ϕ was measured down to 22 eV, but the sensitivity for calculating n and k was poor in the energy region 22 to 33 eV, and therefore the directly measured R_n was considered more reliable in this energy region. Representative data showing how an adenine film can change with time are shown in Figure 8.

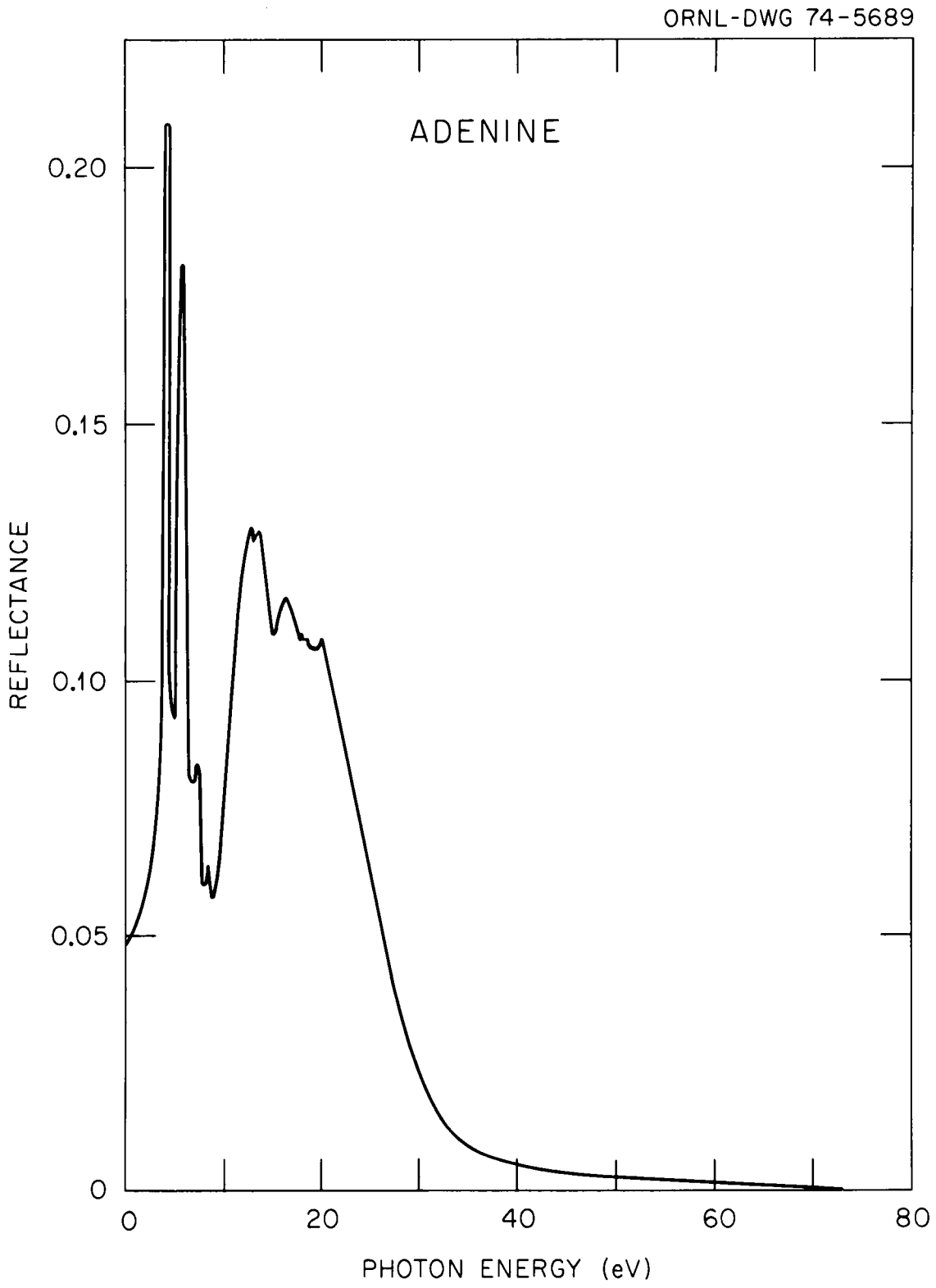

Figure 7. Near-normal incidence reflectance of adenine films as a function of incident photon energy.

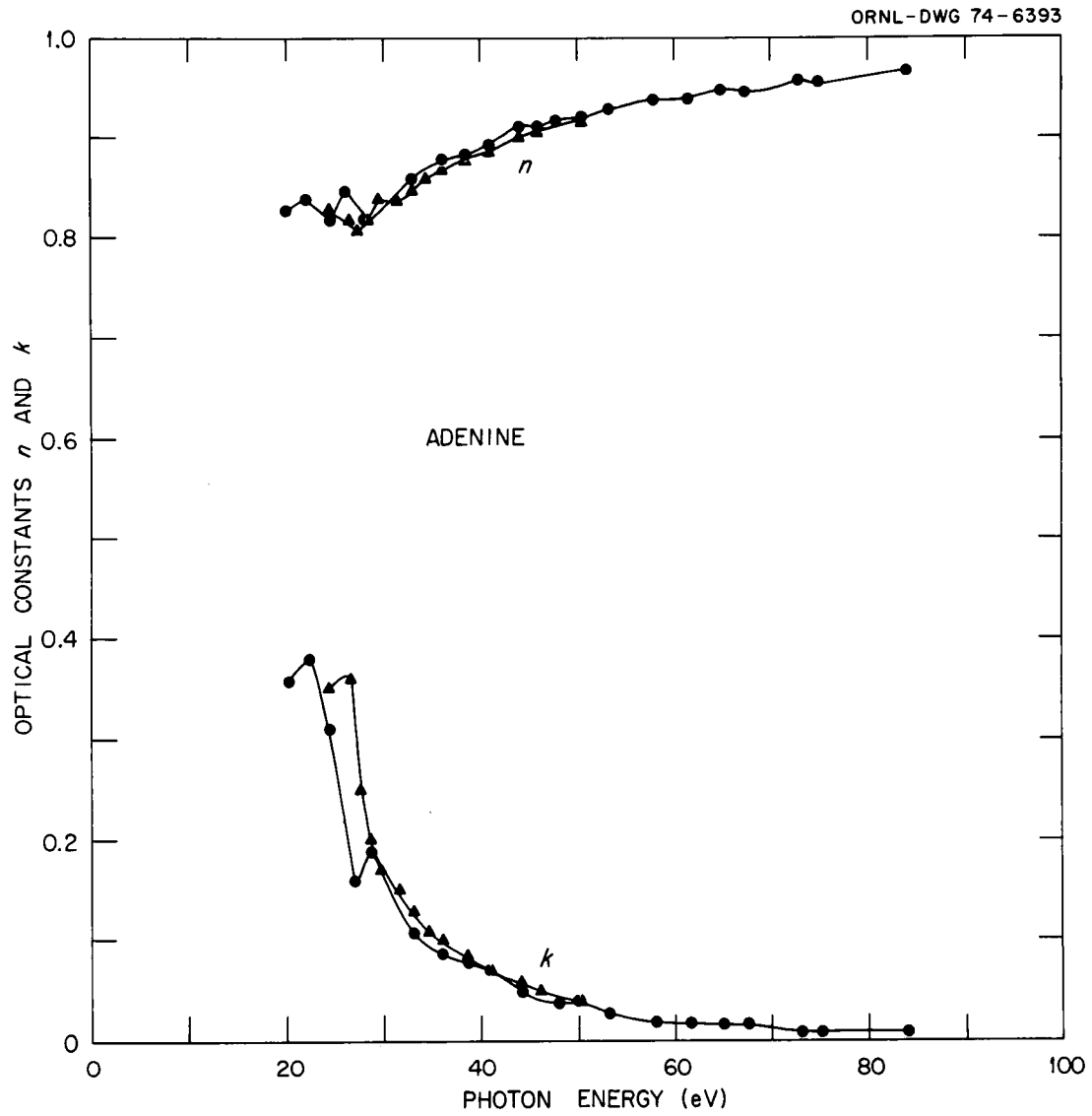

Figure 8. The real and imaginary parts n and k of the refractive index of adenine as a function of incident photon energy.

(The two curves are measurements on the same film taken at different times. ▲ several hours old; ● four days old.)

The measured values of n and k from 2 to 4.2 eV and 33 to 82 eV were then used together with R_n from 2 to 82 eV in a Kramers-Kronig analysis. For each energy where n and k were measured, the phase change on reflection, $\Delta\theta(E)$, due to absorptive processes from 82 eV to infinite energy, was calculated. To do this the measured reflectance, R_n, was extrapolated to zero energy and the integral $\theta_{KK}(E)$ in Equation (36) evaluated numerically over the energy range 0 to 82 eV. The total phase change $\theta(E)$ was calculated from Equation (37). Knowing both $\theta_{KK}(E)$ and $\theta(E)$, the quantity $\Delta\theta(E)$ was then calculated by substitution in Equation (36), and is plotted in Figure 9. Various smoothly varying monotonic interpolations were tried for $\Delta\theta(E)$ in the energy region from 4.2 to 33 eV. The one used, and shown in Figure 9, makes the sum rules, Equations (38) and (39), saturate at the same number of electrons/molecule. The values of $\Delta\theta(E)$ in Figure 9 were then substituted in Equation (36) together with the corresponding values of $\theta_{KK}(E)$ to yield $\theta(E)$ over the energy range from 2 to 82 eV. The optical constants n and k were then calculated from Equations (33), and are shown in Figure 6, page 36. In this way the optical constants n and k were obtained for adenine over the whole experimental range from 0 to 82 eV.

Kramers-Kronig analyses of R_n from 0 to 82 eV were also performed by hypothesizing an analytic form for R_n above 82 eV and then performing the integral [Equation (34)] for the phase change directly. Both an exponential and a power law function were used. The adjustable parameters in the functions were chosen such that the resulting optical constants matched the measured

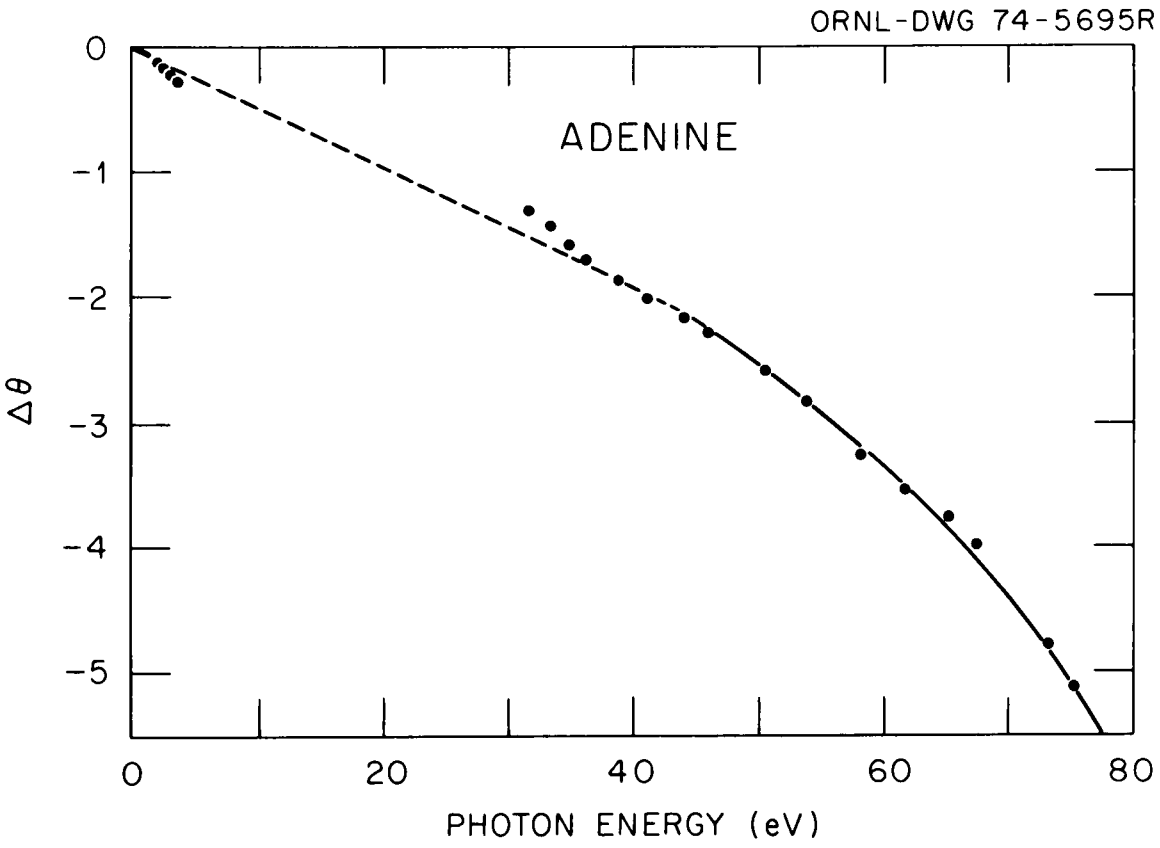

Figure 9. Contribution to the phase change on reflection due to absorption in the energy region above 82 eV for adenine as a function of incident photon energy.

values at both low and high energies. The results obtained by all three Kramers-Kronig calculations were in agreement with each other over the whole range of experimental energies. It is of interest that the best fit for the power law extrapolation gave $R \alpha E^{-4}$, which is the theoretical variation for metals at sufficiently high energies. This confirms previous observations [Williams et al. (1974)] that molecular liquids and solids, such as adenine, show metallic-like behavior at energies sufficiently above the energies of the $\pi \rightarrow \pi^*$, $\sigma \rightarrow \sigma^*$, etc., molecular excitations.

Cytosine, Thymine, and Uracil

For cytosine, thymine, and uracil the only measurements in this study were in the energy region from 22 to 82 eV. Reflectance as a function of angle of incidence from 50° to 86° was measured and n and k extracted at each photon energy using a two-parameter least squares fit to Equation (29) with $d = \infty$. Values obtained for the optical functions are presented in Figure 10 for cytosine, Figure 11 for thymine, and Figure 12 for uracil.

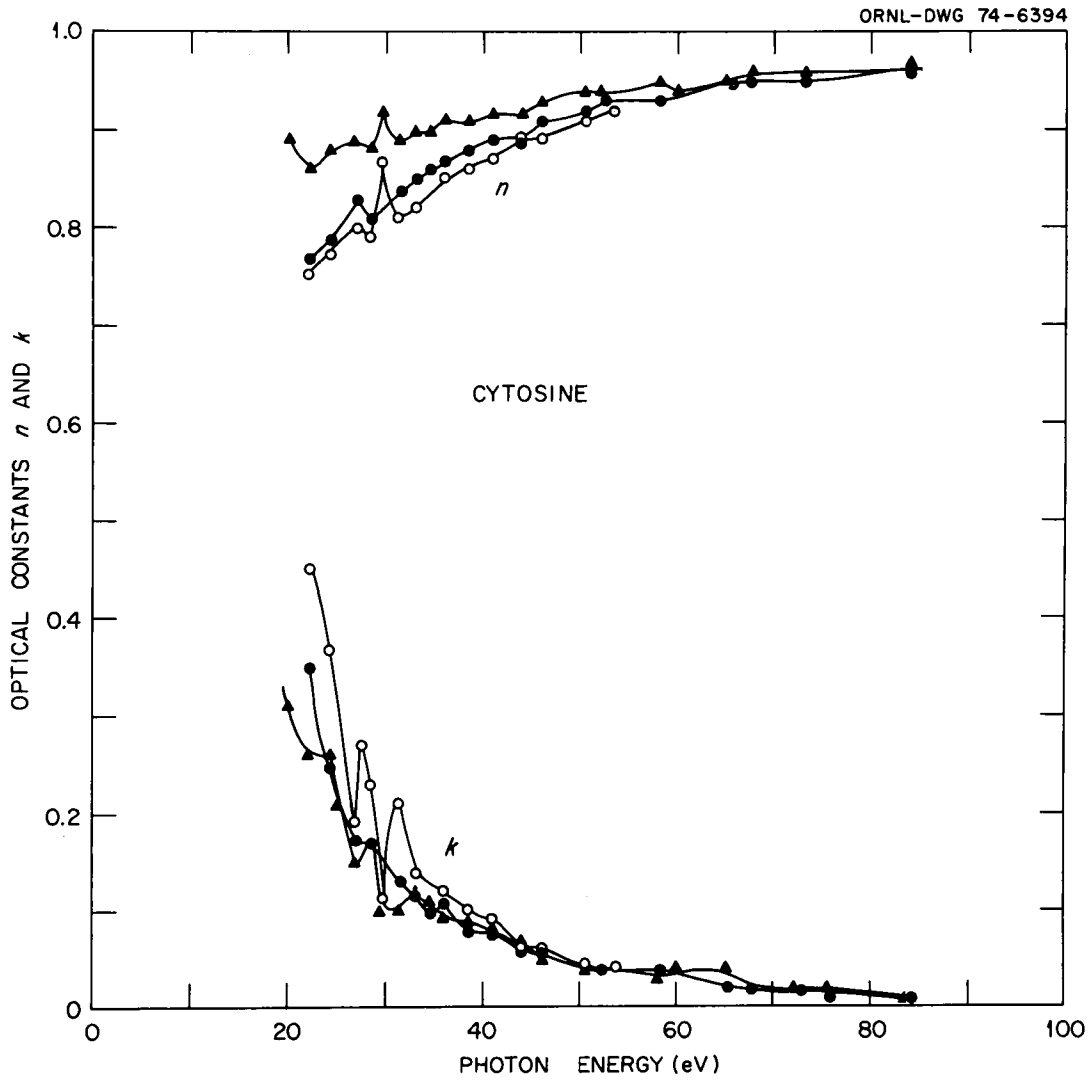

Figure 10. The real and imaginary parts n and k of the refractive index of cytosine as a function of incident photon energy.

[The three curves are measurements on two different films, i) o, ii) • a few hours old, ▲ four days old.]

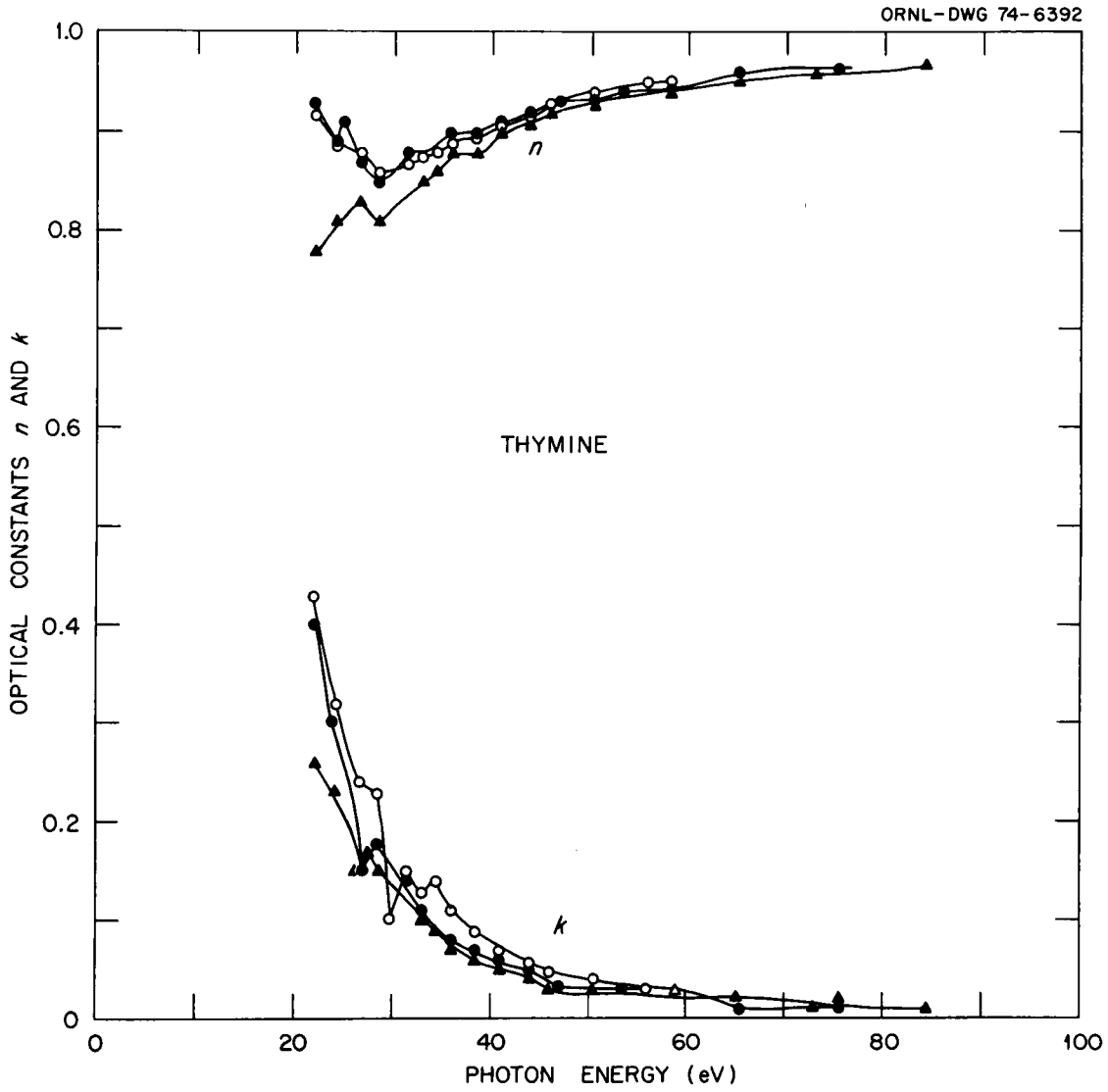

Figure 11. The real and imaginary parts n and k of the refractive index of thymine as a function of incident photon energy.

(The three curves are measurements on three different films.)

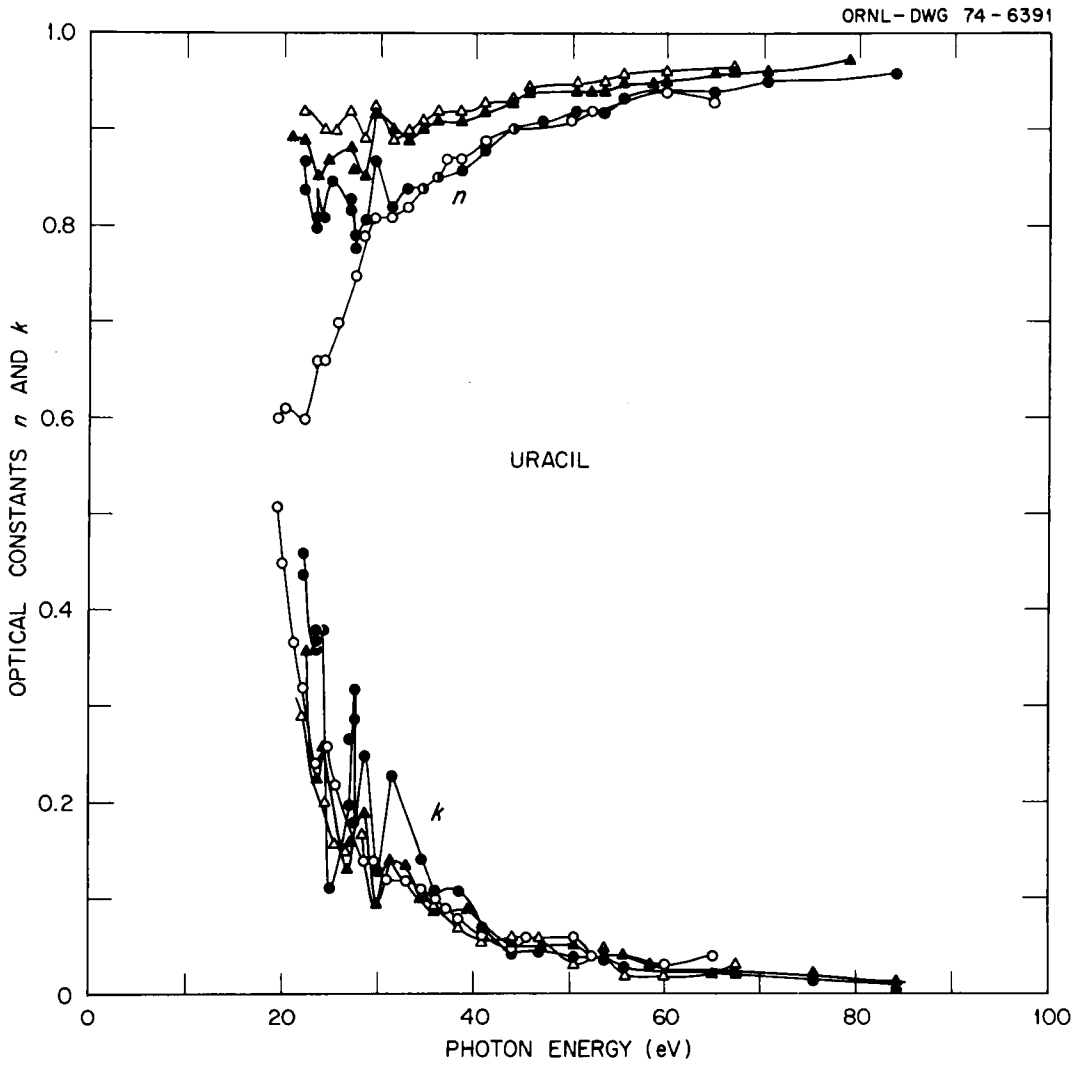

Figure 12. The real and imaginary parts n and k of the refractive index of uracil as a function of incident photon energy.

(The four curves are measurements on four different films.)

CHAPTER V

RESULTS AND DISCUSSION

I. ADENINE

The optical properties of adenine obtained from this study have been presented in Figure 6, page 36, in the form of the real and imaginary parts n and k, respectively, of the complex refractive index, $\tilde{n}$. For comparison with previously published data on adenine (Table I) the k values between 4 and 10 eV from Figure 6 are plotted in Figure 13 along with the values obtained from transmission measurements by Tang et al. (1973). It is seen that there is general agreement, both in the magnitude of k and in the positions of the main peaks. The only other comparable data [Yamada and Fukutome (1968) and Onari and Watanabe (1970), see Table I], on thin films of adenine over the energy range from 4 to 10 eV, were not plotted in Figure 13 since these authors do not present absolute k values. The absorption peak positions of the present study and those of the previous transmission studies of Tang et al. (1973) and Yamada and Fukutome (1968) are compared in Table II. Small differences between corresponding peak positions may be caused by inhomogeneities in one or several of the films or exposure to high humidity conditions after being taken out from the vacuum chamber. It is also possible that the observed differences arise from differences in the

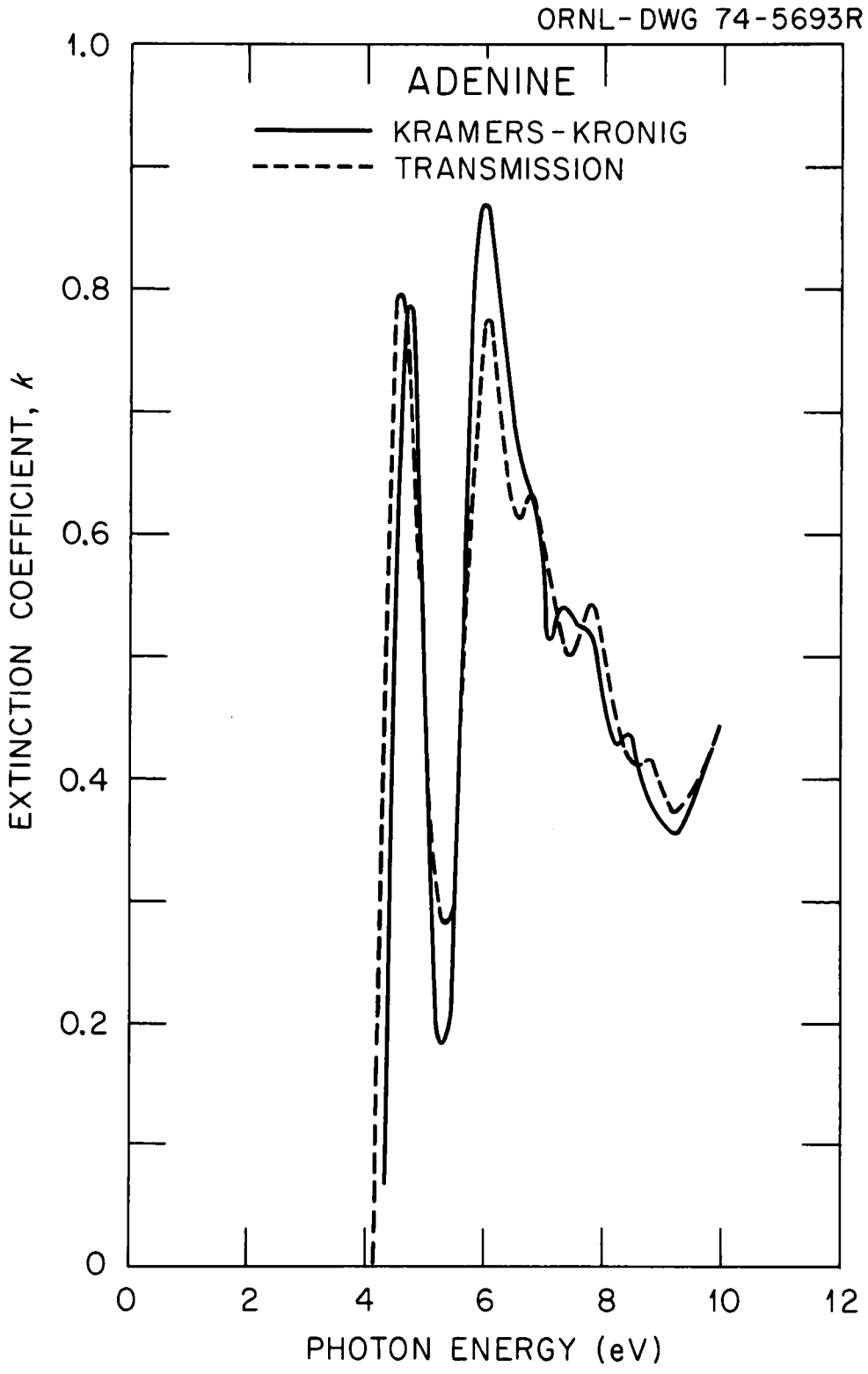

Figure 13. The extinction coefficient, k, of adenine as a function of incident photon energy compared with the values obtained by Tang et al. (1973) from transmission measurements.

TABLE II

COMPARISON OF THE ABSORPTION PEAK ENERGIES

FOR SUBLIMED ADENINE FILMS

Present work (eV)	Tang et al. (1973) (eV)	Yamada and Fukutome (1968) (eV)
4.7	4.57	4.61 - 4.56
5.9	6.02	5.90
7.3	6.78	6.81
7.7	7.75	7.75
8.4	8.70	8.55
		8.86

techniques of sample preparation as the state of the sample has a direct influence on reflectance measurements.

The values of n and k shown in Figure 6, page 36, were used to calculate $\epsilon_1 = n^2 - k^2$ and $\epsilon_2 = 2nk$, where ϵ_1 and ϵ_2 are the real and imaginary parts, respectively, of the complex dielectric function, ϵ. The values of ϵ_1 and ϵ_2 obtained in this way are shown in Figure 14 while the corresponding energy loss function, $-\text{Im } 1/\epsilon$, is shown in Figure 15.

Examination of the experimental spectrum for ϵ_2 in Figure 14 shows that peaks occur at 4.6, 5.8, 7.3, 8.4, and 12.6 eV and shoulders at 6.8, 9.7, and 15.5 eV for our solid films of adenine. These energies are very close to the excitation energies of the allowed electron transitions in the solid. Actually allowed transitions occur at energies given by maxima in the optical conductivity $\sigma = E\epsilon_2/2h$ [Moss (1961), and Frŏhlich and Pelzer (1955)]. In the region of the spectrum (0-7 eV) where we can compare experiment with theory the positions of the peaks in ϵ_2 and σ essentially agree.

Many attempts have been made to calculate theoretically the energies of possible electronic transitions in an adenine molecule. Recent calculations are due to Tanaka and Nagakura (1966), Berthod et al. (1966, 1967), Kuprievich (1967), Mely and Pullman (1969), Packer et al. (1969), Bailey (1970), Šubertová (1973), and Hug and Tinoco (1973, 1974). Each author gives extensive references to previous work reported in the literature.

Tanaka and Nagakura (1966) measured the near and vacuum ultraviolet spectra of adenine, using an evaporated film of adenine on quartz and also

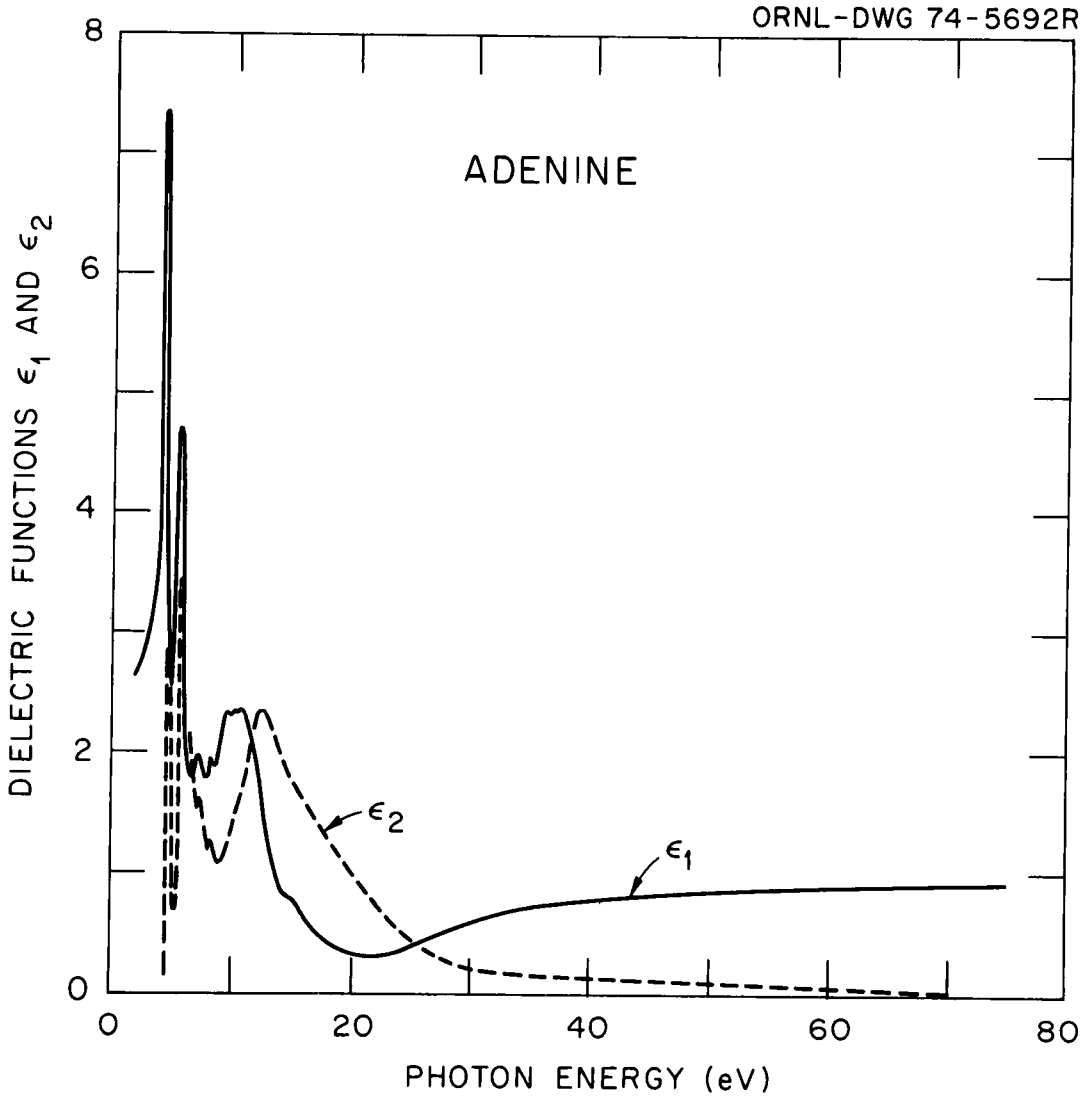

Figure 14. The real and imaginary parts ϵ_1 and ϵ_2 of the complex dielectric constant ϵ of adenine as a function of incident photon energy.

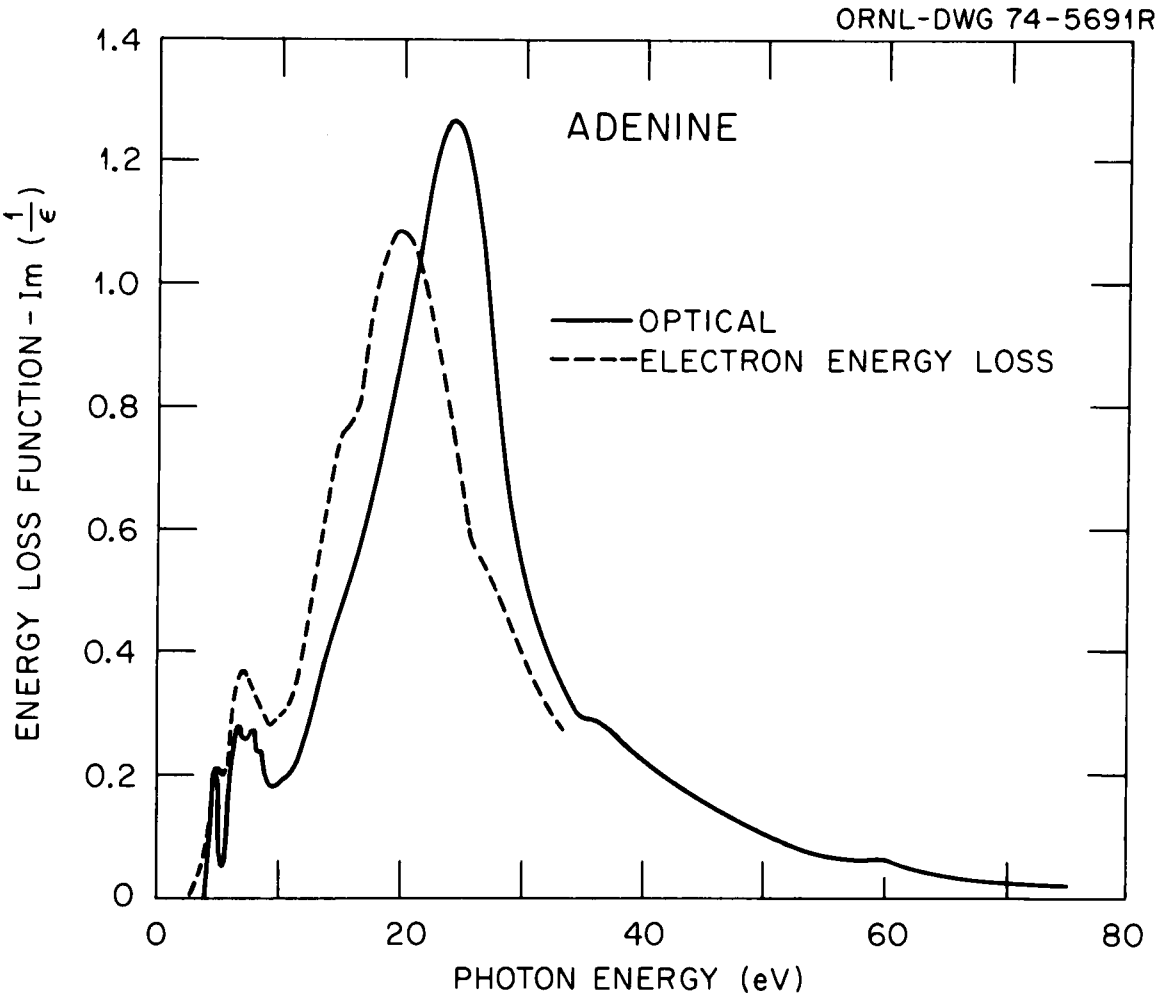

Figure 15. Energy loss function, $-\mathrm{Im}(1/\epsilon)$, of adenine as a function of incident photon energy.

a solution of adenine in water (Table I, page 5). They then made assignments of the absorption bands by comparing the observed transition energies and intensities with the theoretical results obtained by a semi-empirical linear combination of atomic orbitals-self consistent field-configuration interaction (LCAO-SCF-CI) method. They observed transition energies at 4.61, 4.73, 5.98, 6.77, and 7.56 eV and calculated the energies to be at 4.45, 4.81, 5.61, 6.77, 6.90, 7.15 and 7.42 eV. Thus their experimental and theoretical results showed good agreement. Furthermore, they showed apparently for the first time, that the transitions observed in this energy region were all due to $\pi \rightarrow \pi^*$ excitations.

Bailey (1970) discusses the semi-empirical SCF calculations of Berthod et al. (1966, 1967) which include the effects of configuration mixing. In the calculations of Berthod et al. the observables used were ionization potentials and dipole moments, as well as absorption spectra. Bailey calculated the absorption spectrum of adenine without recourse to the experimental spectra of the bases, and then made a comparison with experiment. In a variant of the Pariser-Parr-Pople, PPP-MO, method using a combination of Slater orbitals for the π-electrons, Bailey obtained transition energies of 4.69, 4.87, 5.89, 6.01, 6.24, 6.83, 6.89, 7.28, and 7.79 eV compared with the values of 4.8, 5.0, 5.8, 6.3, 6.5, and 6.9 eV obtained by Berthod et al. This method thus gave good agreement with experimental spectra (see Table I, page 5). The importance of Bailey's presentation was that experimental absorption spectra are not required to parameterise the calculations for molecules of biological interest, such as adenine.

Šubertová et al. (1973) obtain an energy diagram of adenine from observations of the photoemission threshold, the quantum efficiency threshold of photoconductivity, and the polarization energy as calculated from the low frequency permittivity, but the agreement with experiment is not good.

The calculations which include all the electrons, n, π, and σ are those of Mely and Pullman (1969) and Hug and Tinoco (1973, 1974). Mely and Pullman in a non-empirical SCF-MO calculation obtained both occupied and virtual molecular orbital energies for the adenine molecule. Because of the non-empirical nature of the calculations, however, only relative differences between energy levels have meaning. They did show the π and σ levels are inter-mixed to a large extent in the intermediate energy region, while at sufficiently high energies $\sigma \rightarrow \sigma^*$ excitations predominate. The most recent, known, calculations for adenine are due to Hug and Tinoco (1973, 1974). They used an all valence electron SCF-MO method which included configuration interaction for the excited states, and found transition energies at 4.77, 5.03, 5.60, 6.74, 6.89, 7.04, and 7.49 eV. When they assign half widths to these transitions they get broad peaks in their calculated spectrum for adenine at 4.85 and 7.0 eV. Although σ electrons are included in the calculations, all of the transitions in this energy region are shown to be $\pi \rightarrow \pi^*$ excitations.

The general agreement between the energies of the theoretically derived molecular excitations and the structure which we observe in ϵ_2 for solid adenine indicates that adenine behaves as a molecular solid in which the molecular energy levels are only slightly perturbed by the proximity of other molecules.

Isaacson (1972) draws an energy level diagram from the analysis given by Mely and Pullman (1969). From this, and the other theoretical papers quoted above, we conclude that the structures we see in ϵ_2 at 4.6, 5.8, 6.8, and 7.3 eV correspond to $\pi \rightarrow \pi^*$ excitations, while those at 12.6 and 15.5 eV correspond to $\sigma \rightarrow \sigma^*$ excitations. The structures at 8.4 and 9.7 eV are in the intermediate energy region and remain unidentified.

The directly measured spectrum above 10 eV is presented for the first time and could be the basis for extending the theoretical calculation of the electronic states in adenine to higher energies than has been possible to date.

Electron energy loss measurements for adenine using a scanning electron microscope (SEM) equipped with a high resolution magnetic spectrometer have been reported by Isaacson (1972). Eventually the aim is to refine this method so that the sequence of bases in a particular DNA molecule will be identifiable from the spectra of the individual bases. In fact, it is hoped that even atomic arrangement within the organic molecule itself will be identifiable by this technique. However, it has been conjectured that the results obtained might be affected by radiation damage caused by the electron beam. Isaacson calculated values for the dielectric functions ϵ_1 and ϵ_2 and the energy loss function -Im $1/\epsilon$ from his electron energy loss measurements, after correcting for multiple scattering of the high energy electrons. One purpose of the present measurements was to compare our optically measured ϵ_1, ϵ_2, and -Im $1/\epsilon$ with the calculated values obtained by Isaacson. Any

disagreement between corresponding quantities can be caused by i) the experimental resolution attainable in the two experiments, ii) the uncertainty in the derivation of ϵ_1 and ϵ_2 from the electron energy loss spectra, iii) radiation damage inflicted to the adenine by the incident photons and/or high energy electrons, and iv) possible inaccuracies, including such things as film quality, in either experiment. The values of $-\mathrm{Im}\ 1/\epsilon$ calculated by Isaacson are plotted in Figure 15, page 51, for comparison with our values, and it is seen that there is general agreement.

Several things must be taken into consideration when comparing optical spectra with the corresponding energy loss spectra [Powell (1969)]. Since the optical constants n(E) and k(E) are related to the complex dielectric constant $(E,\ \Delta \vec{p} \sim 0)$, where Δp is momentum change, the energy loss function $-\mathrm{Im}[1/\epsilon(E,0)]$, calculated from the optical data corresponds to a "zero-angle" electron energy loss spectrum. If the extent of the experimental angular integration has not been adequately specified, electron energy loss spectra cannot be compared in detail with optically determined $\mathrm{Im}[1/\epsilon(E,0)]$ spectra. In addition, corrections due to multiple inelastic scattering and to the excitation of multiple plasmon losses must be made when it is desired to determine $\mathrm{Im}[1/\epsilon(E,0)]$ from transmission electron energy loss spectra. Optimum specimen thickness should be chosen to minimize these corrections.

In the electron energy loss experiments for adenine [Isaacson (1972)], the incident beam aperture and the analyzer aperture subtended a half angle of

0.625 mrad. This aperture size was approximately equal to, or smaller than, the characteristic inelastic angle $\theta_E = E/2E_o$ for all energy losses E. Thus this could be considered as a zero-angle electron energy loss distribution. Corrections were made only for double inelastic scattering, but for the film thickness and experimental apparatus they were using, triple and higher order inelastic scattering could be neglected. With these corrections made by Isaacson, we should be able to compare his final -Im $1/\epsilon$ spectrum directly with that from our optical measurements. Examination of the two curves in Figure 15, page 51, shows that the positions of the main peaks in $-\mathrm{Im}(1/\epsilon)$ do not appear to be limited by lack of resolution of either apparatus. At low energies (0 - 10 eV) the resolution associated with the optical data appears to be greater than that associated with the electron energy loss data.

The most significant difference between the energy loss function obtained in the present study and that from the SEM study lies in the energy at which the high energy loss peak occurs. As seen in Figure 15 the present results indicate a sharp peak at $\sim$ 24 eV whereas the SEM results exhibit an equally sharp peak at $\sim$ 20 eV. The same sort of discrepancy has been noted by Emerson et al. (1974) for guanine. In the case of guanine it was suggested that the difference in the peak energies resulted from the use of smoother films (higher specular reflectance at a given photon energy) in the optical studies than in the SEM studies. The possibility of such a large discrepancy being caused by radiation damage is ruled out by the studies of Isaacson et al. (1973) on radiation damage to adenine films. These studies showed that

radiation damage results in a general degradation of the adenine $-\mathrm{Im}(1/\epsilon)$ spectrum which is not seen in either spectrum in Figure 15, page 51, This conclusion is also confirmed by Isaacson et al. (1973) who calculated that radiation damage should be negligible at the dose levels used in the SEM studies. Finally reasonable estimates of the maximum possible experimental errors in ϵ_1 and ϵ_2 in the region of 20 - 25 eV give $\pm$ 10% in the optical studies and $\pm$ 15% in the SEM studies. The observed difference in the peak positions is greater than can be accounted for by such experimental errors. Thus, as with guanine, we suggest that the difference between the positions of the high energy peaks in $-\mathrm{Im}(1/\epsilon)$ for adenine, as shown in Figure 15, is real and is due to differences in the films used in the two studies.

The energy loss function spectrum for adenine (Figure 15) calculated from our optical measurements, shows structure that can be correlated with the structure in ϵ_2 (Figure 14, page 50). We have already associated the peaks in ϵ_2 with $\pi \rightarrow \pi^*$ and $\sigma \rightarrow \sigma^*$ molecular excitations. Peaks in the energy loss function are shifted to energies higher than the corresponding optical transitions [Williams et al. (1974)]. The magnitude of this shift gives some qualitative indication of the degree of collective effects associated with a particular peak although it does not permit one to say how much of a particular transition is "collective" or "non-collective" in nature. Thus each peak in $-\mathrm{Im}(1/\epsilon)$ can be associated with the corresponding molecular excitation plus a collective electron loss directly related to the energy shift between the peak

in $-\mathrm{Im}(1/\epsilon)$ and the corresponding peak in ϵ_2. The collective effects are hybrid resonances rather than the totally free electron resonances seen in nearly-free-electron-like metals. However, both the hybrid and nearly-free-electron resonances occur when the magnitudes and energy variations of the dielectric functions show similar properties suitable for sustaining collective oscillations (see Chapter II, page 24).

The peaks seen in $-\mathrm{Im}(1/\epsilon)$ at 4.9, 6.9, 7.85, 8.45, and 24 eV (optical values Figure 15, page 51) correspond to the peaks in ϵ_2 at 4.6. 5.8, 7.3, 8.4, and 12.6 eV. Thus the two peaks in $-\mathrm{Im}(1/\epsilon)$ showing the greatest degree of collective effects are those at 6.9 eV, involving only the π electrons, and at 24 eV, involving all the valence electrons.

The sum rules as given in Equations (38) and (39) were used to calculate, respectively, the effective number of electrons per molecule contributing to optical transitions and to the electron energy loss up to an energy E_o. The results of these calculations are shown in Figure 16. Both curves are almost saturated by 75 eV at 46.3 electrons, using our measured density of 1.35 gm-cm^{-3} in the calculations. The number of valence electrons in an adenine molecule is 50; thus the oscillator strengths are essentially exhausted at 75 eV.

We obtained the density of our films by independent measurements of the mass and thickness of a film deposited on a quartz substrate of known area. The film thickness was determined from the fringe spacing in the reflectance spectrum in the region where the film is transparent. The mass was

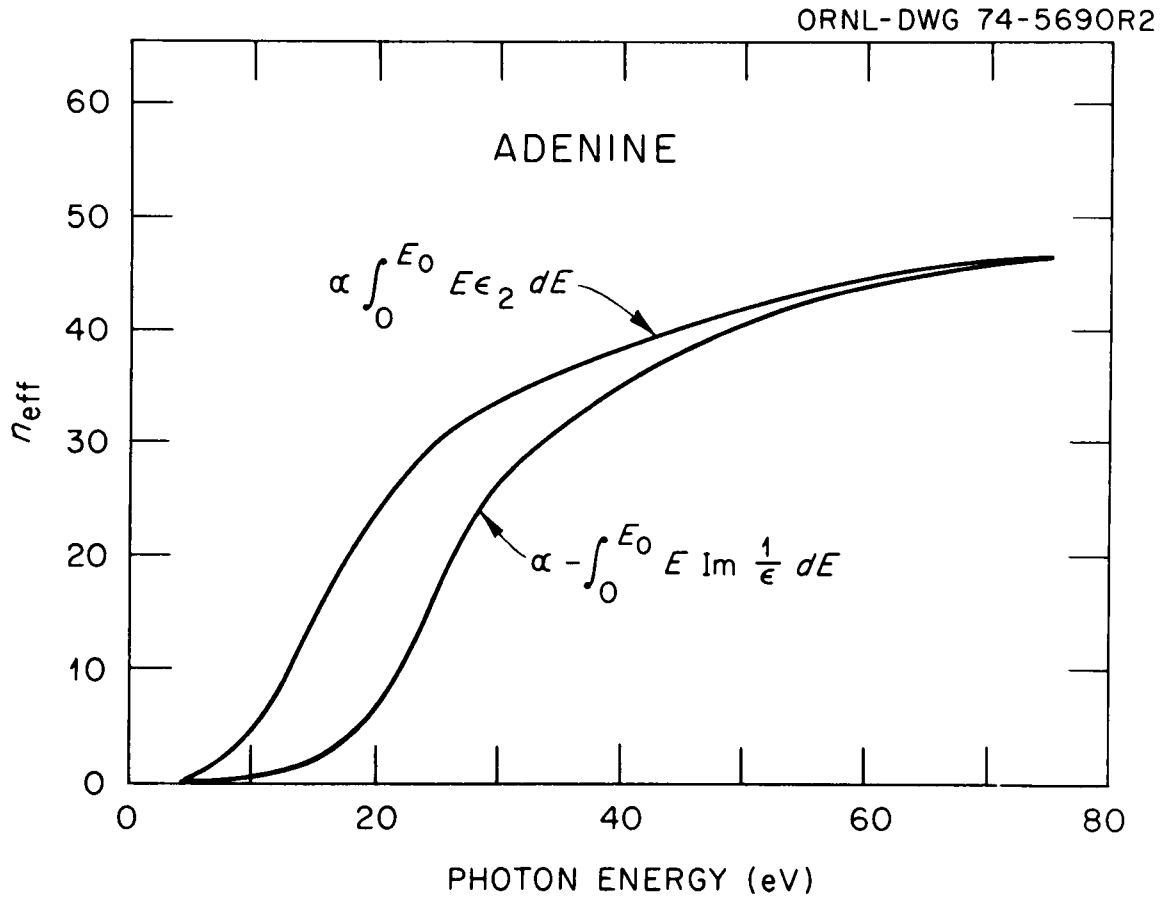

Figure 16. The effective number of electrons participating in optical excitations [$n_{eff}(\epsilon_2)$] and the effective number of electrons participating in energy losses [$n_{eff}(\mathrm{Im}(1/\epsilon))$] in adenine up to an incident photon energy E_0.

determined by dissolving the film in 0.1 N HCl and measuring the absorbance A at 2600 Å using a 1 cm quartz transmission cell. The concentration (and hence the mass) was obtained from the relation $C = AM/(\epsilon \ell)$ where M is the molecular weight, ℓ the optical path length and ϵ the molar absorptivity for the peak at 2600 Å which was taken to be 1.31×10^4 cm^2/mole [Thomas (1952)]. From this method the film density was found to be 1.35 gm/cm^3. An independent determination of the mass was obtained with a quartz crystal film thickness monitor calibrated for aluminum. Agreement to within one percent was obtained by the two methods. The density of compact microcrystals of adenine has also been determined by Šubertová et al. (1973). Using benzene, in which adenine is practically insoluble, as a pycnometric fluid they determined a density of (1.48 ± 0.03) $gm\text{-}cm^{-3}$. Isaacson (1972) using a normalization technique based on the sum rules, found a density of 1.31 $gm\text{-}cm^{-3}$ while Voet and Rich (1970) measured a value of 1.44 $gm\text{-}cm^{-3}$ for single crystals.

II. CYTOSINE, THYMINE, AND URACIL

Figures 10-12, pages 43-45, respectively, show the optical functions for cytosine, thymine, and uracil measured on different films. In some cases, as indicated in the figure captions, the effect of aging is seen in the values of the constants. For the freshly deposited films the average values of the optical constants at each photon energy were used to calculate ϵ_1, ϵ_2, and $-\mathrm{Im}(1/\epsilon)$. The values obtained for cytosine, thymine, and uracil are shown in Figures 17-19.

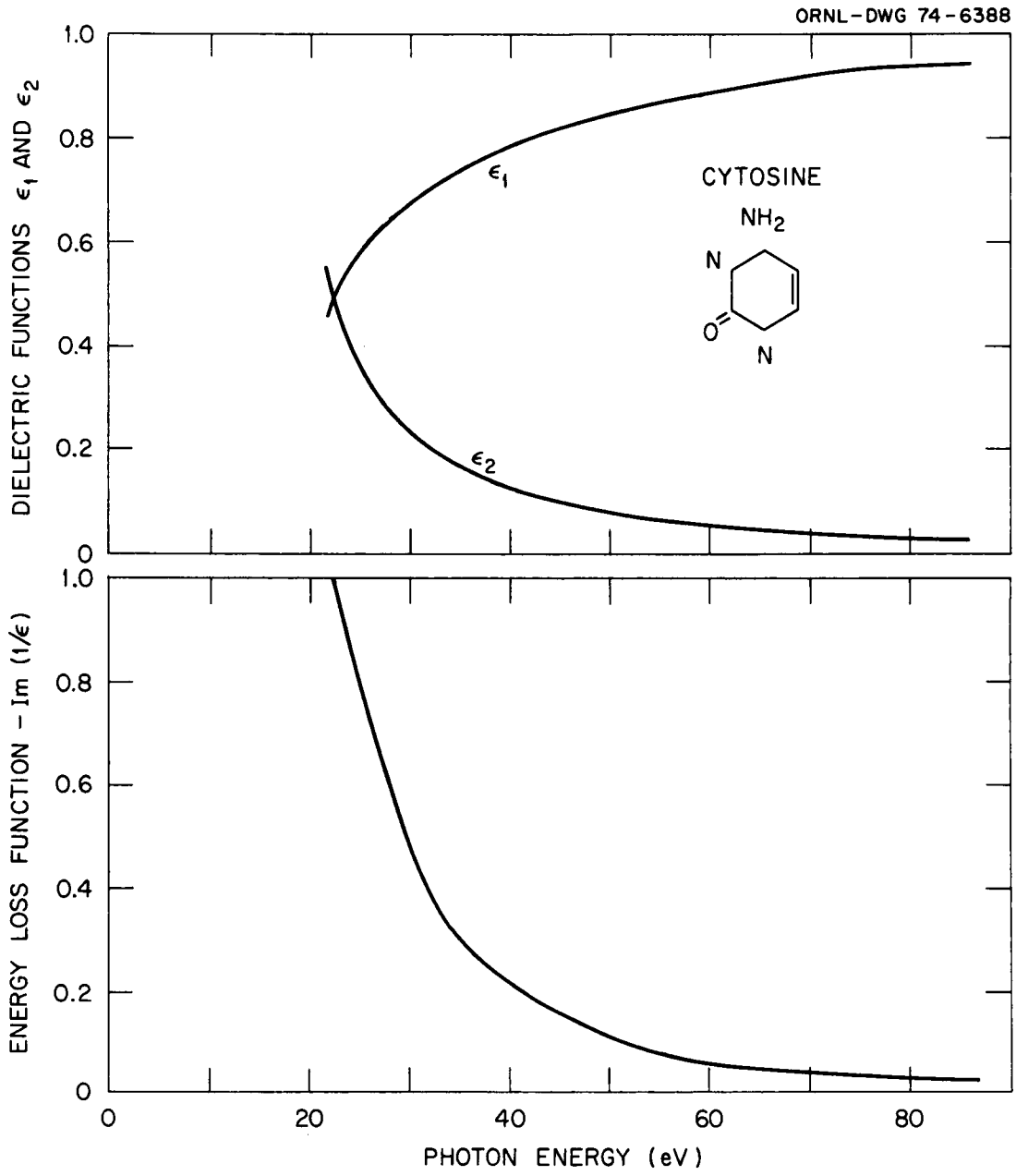

Figure 17. The real and imaginary parts ϵ_1 and ϵ_2 of the complex dielectric constant ϵ and the energy loss function, $-\mathrm{Im}(1/\epsilon)$, of cytosine as a function of incident photon energy.

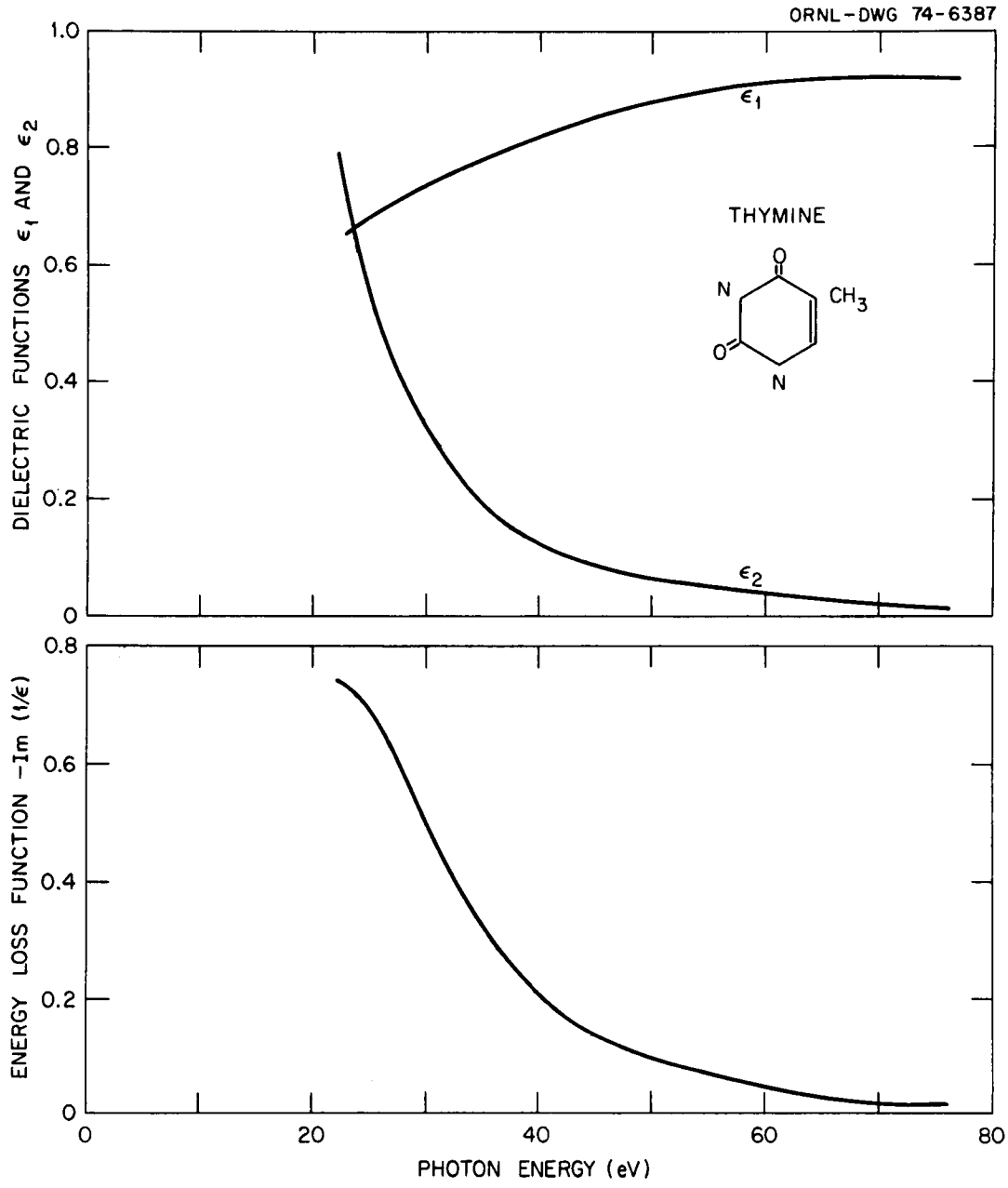

Figure 18. The real and imaginary parts ϵ_1 and ϵ_2 of the complex dielectric constant ϵ and the energy loss function, $-\mathrm{Im}(1/\epsilon)$, of thymine as a function of incident photon energy.

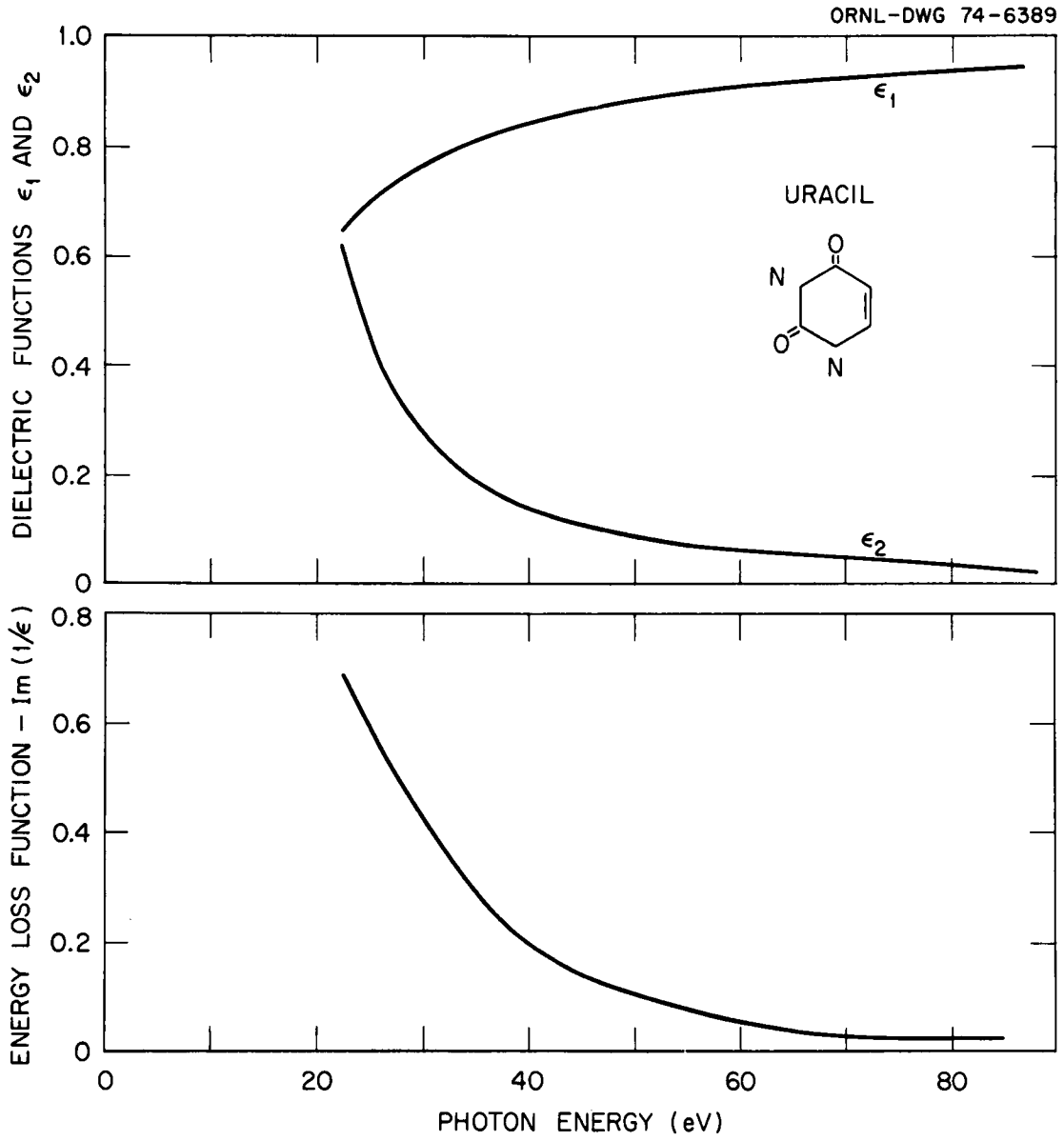

Figure 19. The real and imaginary parts ϵ_1 and ϵ_2 of the complex dielectric constant ϵ and the energy loss function, $-\mathrm{Im}(1/\epsilon)$, of uracil as a function of incident photon energy.

CHAPTER VI

SUMMARY

The optical properties of the nucleic acid bases adenine, thymine, cytosine, and uracil were studied as functions of energy in the range 2 to 82 eV for adenine and 25 to 82 eV for the rest. The optical properties, the complex refractive index $\tilde{n}$ and the complex dielectric constant ϵ, can be related to the electronic structure of each biological molecule and the energy loss properties of the material. Reflectance measurements from thin films on glass provided the basic data used in all calculations in this study where the thin films were vacuum deposited on the glass. Fresnel's equations and a Kramers-Kronig analysis were used to obtain $\tilde{n}$ and ϵ from the reflectance data for adenine.

The optical properties found for adenine were compared with other experimental data and theoretical calculations. Comparison of k, the imaginary part of $\tilde{n}$, with those values measured in the previous studies, gave good agreement. Acceptable agreement was also found between theoretically derived molecular excitations and peaks in ϵ_2, the imaginary part of ϵ. It was possible on the basis of this to correlate some of the peaks with $\pi \rightarrow \pi^*$ and $\sigma \rightarrow \sigma^*$ transitions. A comparison of the energy loss function, $-\mathrm{Im}(1/\epsilon)$, with energy losses observed in scanning electron microscope experiments was also made. The agreement here was good at low energies but at higher energies the main peak obtained by the two methods differed by 4 eV. This is tentatively explained in terms of differences in film preparation. Finally a comparison of ϵ_2 and

$-\mathrm{Im}(1/\epsilon)$ for adenine shows proper agreement, with an expected shift in peaks due to the presence of collective oscillations of the loosely bound electrons in adenine.

BIBLIOGRAPHY

BIBLIOGRAPHY

Bailey, M. L., Theor. Chim. Acta 16, 309-315 (1970).

Berthod, H., C. Giessner-Prettre, and A. Pullman, Theor. Chim. Acta 5, 53-68 (1966).

Berthod, H., C. Giessner-Prettre, and A. Pullman, Int. J. Quant. Chem. 1, 123-137 (1967).

Bode, H., Network Analysis and Feedback Amplifier Design (D. Van Nostrand Co., Inc., Princeton, 1945), pp. 322-340.

Clark, L. B., G. G. Peschel, and I. Tinoco, Jr., J. Phys. Chem. 69, 3615-3618 (1965).

Ehrenreich, H., and H. R. Phillipp, in Proceedings of the International Conference of the Physics of Semiconductors, ed. by A. C. Strickland (Bartholomew Press, Dorking, England 1962), pp. 367-374.

Emerson, L. C., M. W. Williams, I. L. Tang, R. N. Hamm, and E. T. Arakawa, Optical Properties of Guanine from 2 to 82 eV, Submitted for publication in Radiation Research.

Fenton, E. W., Phys. Rev. 174, 517 (1965).

Frohlich, H., and H. Pelzer, Proc. Phys. Soc. London A68, 525 (1955).

Hoffman, T. A., and J. Ladik, in "The Structure and Properties of Biomolecules and Biological Systems," Vol. VII of Advances in Chemical Physics, ed. by J. Duchesne (John Wiley and Sons, New York 1964).

Horton, V. G., E. T. Arakawa, R. N. Hamm, and M. W. Williams, Applied Optics 8, 667 (1969).

Hug, W., and I. Tinoco, Jr., J. Am. Chem. Soc. 95, 2803-2813 (1973).

Hug, W., and I. Tinoco, J. Am. Chem. Soc. 96, 665 (1974).

Hunter, W. R., J. Opt. Soc. Am. 55, 1197 (1965).

Inagaki, T., R. N. Hamm, E. T. Arakawa, and L. R. Painter, Optical Properties of DNA in the Extreme Ultraviolet. Accepted for publication in J. Chem. Phys. (1974).

Isaacson, M., J. Chem. Phys. 56, 1803 (1972).

Isaacson, M., D. Johnson, and A. V. Crewe, Rad. Res. 55, 205-224 (1973).

Johnson, D. C., Rad. Res. 49, 63 (1972).

Kleinwachter, V., J. Drobnik, and L. Augenstein, Photochemistry and Photobiology 6, 133 (1967).

Kloos, T., Z. Physik 210, 303 (1968).

Kuprievich, V. A., Int. J. Quant. Chem. 1, 561-575 (1967).

Ladik, J., Int. J. Quantum Chem. 4, 307 (1971).

MacRae, R. A., E. T. Arakawa, and M. W. Williams, Phys. Rev. 162, 615 (1967).

Mely, B., and A. Pullman, Theoret. Chim. Acta. (Berlin) 13, 278 (1969).

Moss, T. S., Optical Properties of Semiconductors (Butterworth Scientific Publications, Inc., London 1961).

O'Konski, C. T., P. Moser, and M. Shirai, Biopolymers 1, 479 (1970).

Onari, S., and K. Watanabe, J. Phys. Society Japan 28, 1051 (1970).

Packer, J. C., J. S. Avery, J. Ladik, and G. Biczó, Int. J. Quant. Chem. 3, 79-92 (1969).

Powell, C. J., J. Opt. Soc. Am. 59, 738 (1969).

Preiss, J. W., and R. Setlow, J. Chem. Phys. 25, 138-141 (1956).

Pullman, B., and A. Pullman, Prog. in Nucleic Acid Res and Molec. Biol. 9, 327 (1969).

Rhodes, W., J. Am. Chem. Soc. 83, 3609 (1961).

Ritchie, R. H., Phys. Rev. 106, 874 (1957).

Sinsheimer, R. L., J. F. Scott, and J. R. Loofbourow, J. Biol. Chem. 187, 313-324 (1950).

Snart, R. S., Biopolymers 6, 293 (1968).

Šubertová, E., J. Bok, P. Rahik, V. Prosser, and E. Silinsh, Phys. Stat. Solidi (a) 18, 741 (1973).

Tanaka, M., and S. Nagakura, Theoret. Chim. Acta (Berlin) 6, 320 (1966).

Tang, I. L., E. T. Arakawa, M. W. Williams, R. N. Hamm, L. C. Emerson, and R. D. Birkhoff, "Optical Properties of Nucleic Acid Bases," Oak Ridge National Laboratory Report ORNL-TM-4559.

Thomas, R., Bull. Soc. Chim. Biol. 34, 47 (1952).

Voet, D., W. B. Gratzer, R. A. Cox, and P. Doty, Biopolymers 1, 193-208 (1963).

Voet, D., and A. Rich, Progr. Nucleic Acid Res. Mol. Biol. 10, 183 (1970).

Watson, J. D., and F. H. C. Crick, in Fundamentals of Physical Science (McGraw-Hill, Inc., New York 1971), 6th ed., pp. 568-570 (1953).

Weissbluth, M., Quarterly Rev. of Biophys. 4, 1 (1971).

Williams, M. W., R. N. Hamm, E. T. Arakawa, L. R. Painter and R. D. Birkhoff, Collective Electron Effects in Molecular Liquids, Int. J. Radiation Physics and Chemistry. Accepted for publication in Platzmann Memorial Issue (1974).

Yamada, T., and H. Fukutome, Biopolymers 6, 43 (1968).

VITA

Sung-I Juan was born in Taiwan, Republic of China, on October 7, 1950. She attended Taipei First Girls' High School and was enrolled at Tung-Hai University in 1968. She was awarded a Bachelor Degree of Science with a major in physics in 1972. She then attended the University of Tennessee at Knoxville majoring in health physics. She was employed as a Graduate Assistant during her graduate studies.